monolayer of labeled NECs, and then the adhering ATL cells with labeled NECs were collected after rinsing twice gently with RPMI 1640 medium to remove nonadhering ATL cells. For the proliferation assay, ATL-CR cells were labeled with CFSE and then co-cultured with unlabeled HEK293T cells for 72 hours.[22]

FCM Analysis

Cell-cycle distribution of ATL cells was analyzed by DNA content using the propidium iodide (PI) staining method. Co-cultured cells were harvested after the indicated durations of TSA treatment. After fixation in 70% ethanol at −20°C overnight, cells were incubated in a PI/RNase A staining buffer (50 μg/mL of PI and 20 μg/mL of RNase A in PBS). Cells were then analyzed by FCM using a FACScan flow cytometer (Becton Dickinson, Franklin Lakes, NJ). CFSE and PI were detected in the FL-1 and FL-2 channels, respectively. Co-cultured ATL cells gated on CFSE-negative cells were acquired in 10,000 events. Expression of cell-surface molecules was analyzed using FCM. Analysis was performed using CellQuest Pro software version 6.0 (Becton Dickinson Immunocytometry Systems, San Jose, CA). Sigmoid-like dose-response curves were drawn using the logistic curve-fitting software ImageJ, version 1.46 (NIH, Bethesda, MD).[23]

Immunofluorescence Staining

Cells cultured on chamber slides were fixed with 4% paraformaldehyde for 15 minutes. For intracellular staining, cells were treated with PBS containing 0.1% Triton X-100 (Roche Diagnostics GmbH, Mannheim, Germany) for 4 minutes and then fixed with ice-cold 70% methanol for 4 minutes. Nonspecific binding was blocked with 0.05% Tween 20 in PBS containing 0.1% goat serum for 10 minutes. After incubation with primary antibodies for each targeted protein, Alexa Fluor—conjugated goat polyclonal antibody was used as a secondary antibody. Images were acquired using an Olympus DP70 camera with its own Olympus DP controller software version 1.2.1.108 (Olympus, Tokyo, Japan). Three-dimensional analyses were reconstructed by images acquired by confocal microscopy using a laser scanning confocal microscope (FV-300; Olympus, Tokyo, Japan).

Functional Assays

Reporter genes were introduced into ATL cells directly using FuGENE transfection reagents (Roche Diagnostics, Branchburg, NJ) according to the manufacturer's instructions. Briefly, 5×10^5 ATL-CR cells were cultured in 60-mm dishes and cotransfected with 1 μg of HTLV-1 LTR firefly luciferase reporter plasmid together with 50 ng of the *Renilla* luciferase reporter pRL-TK. Eighteen hours after transfection, ATL-CR cells were washed five times in PBS and then were co-cultured with HEK293T cells in the presence of TSA in triplicate wells of 24-well plates (2×10^5 cells per well). Reporter activities were measured using the Dual-Luciferase reporter assay system (Promega, San Luis Obispo, CA). Briefly, cells were lysed in 1× passive lysis buffer, and firefly and *Renilla* luciferase activities were measured using a Turner 20/20 luminometer (Promega). Reporter activities were normalized using *Renilla* luciferase values.

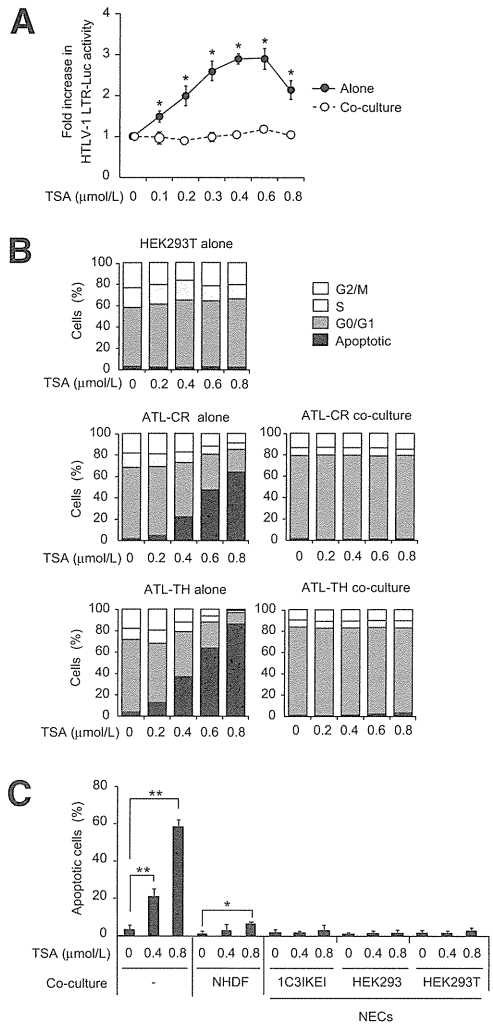

Figure 1 Direct co-culture with NECs rescued ATL cells from TSA-induced apoptosis. **A:** Transcriptional activity of HTLV-1 LTRs in TSA-treated ATL-CR cells. ATL-CR cells were cotransfected with 1 μg of HTLV-1 LTR firefly luciferase reporter plasmid together with 50 ng of pRL-TK 1 day before co-culture with HEK293T cells. After 18 hours of co-culture with the indicated concentrations of TSA, reporter activities were measured and normalized to *Renilla* luciferase values. The values indicate the means ± SD fold increases obtained by three independent experiments normalized to the untreated control sample. **B:** Cell-cycle analysis in ATL-CR and ATL-TH cells. ATL cells, 5×10^5 per well, were cultured alone or with HEK293T cells in the presence of the indicated concentrations of TSA for 48 hours. HEK293T cells were labeled with CFSE 1 day before co-culture. After the whole co-cultured cells were harvested, cell-cycle analysis was performed by FCM. **C:** Percentage of apoptotic ATL-CR cells co-cultured with normal human dermal fibroblasts (NHDFs), 1C3IKEI cells, HEK293 cells, and HEK293T cells. The data are presented as the means ± SD of three independent experiments. $*P < 0.05$, $**P < 0.01$.

Cytotoxicity Assays

Cytotoxicity assays used a combination of two dyes: CFSE was used to label effector cells (KHYG-1 cells) and HEK293T cells and PI was used to stain target cells (ATL-CR cells). CFSE-labeled effector cells were incubated with nonlabeled target cells cultured alone or co-cultured with CFSE-labeled HEK293T cells at effector to target cell ratios of 3:1, 6:1, or 9:1 in triplicate wells of 24-well plates for 18 hours. Apoptotic ATL-CR cells were evaluated by the percentage of sub G0/G1 phase cells in CFSE-negative cells as determined by FCM. Mean values were calculated from three independent experiments.

Statistical Analysis

Data were analyzed using either the Student's t-test or repeated-measures analysis of variance. A $P < 0.05$ was considered statistically significant.

Results

Direct Co-Culture with NECs Rescues ATL Cells from TSA-Induced Apoptosis

HTLV-1 gene expression is hardly detectable in ATL cells because of gene silencing. With the aim of eliminating viral gene silencing, we treated the IL-2–independent ATL-derived cell line ATL-CR with TSA. This treatment increased the amount of HTLV-1 p19 gag protein in the supernatants and lysates prepared from cultured ATL-CR cells (data not shown) and enhanced the transcriptional activity of HTLV-1 LTRs in a dose-dependent manner (Figure 1A), indicating that TSA effectively eliminates viral gene silencing. However, when ATL-CR cells were co-cultured with HEK293T cells (used as NECs), treatment with TSA did not increase the transcriptional activity of HTLV-1 LTRs, indicating that co-culture with NECs blocked TSA-induced viral gene reactivation (Figure 1A).

Next, we performed cell-cycle analysis to determine whether HEK293T cells affect the fate of TSA-treated ATL-CR and ATL-TH cells (Figure 1B). When ATL-CR cells were cultured alone in the presence of TSA, they displayed a dose-dependent increase in the percentage of apoptotic cells and a decrease in the percentage of G0/G1 phase cells; similar changes were observed in TSA-treated ATL-TH cells but not in TSA-treated HEK293T cells. ATL-CR and ATL-TH cells co-cultured with HEK293T cells showed no increase in the percentage of apoptotic cells; instead, the percentage of G0/G1 phase cells was increased. The ability of HEK293T cells to prevent apoptosis was evident even at an ATL-CR to HEK293T cell ratio of 25:1 (data not shown). Similar apoptosis-protective effects were also observed when ATL-CR cells were co-cultured with primary epithelial cells 1C3IKEI or primary dermal fibroblasts (Figure 1C). These results indicate that co-culture with NECs generally prevents ATL cells from TSA-induced apoptosis.

Cell-Cell Contact–Dependent Interactions with NECs Are Required to Rescue ATL Cells from HDAC Inhibitor–Induced Apoptosis

To examine whether cell-cell contact with NECs is required to rescue ATL cells from TSA-induced apoptosis, we co-cultured ATL-CR cells in direct or indirect contact with HEK293T cells in the presence of TSA. When ATL-CR cells were separated by 0.4-μm membranes from HEK293T cells, the ratio of apoptotic ATL-CR cells was lower than when they were cultured alone but showed a marked increase compared with when ATL-CR cells were cultured in direct

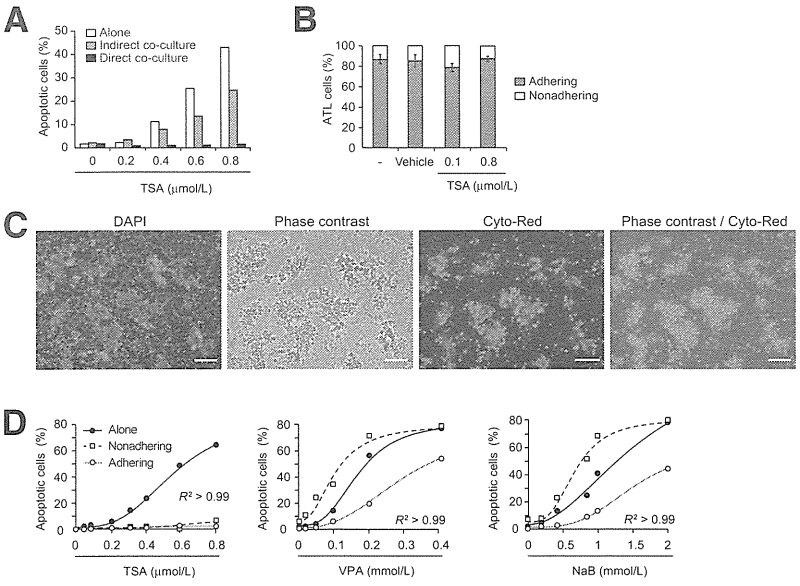

Figure 2 Cell-cell contact–dependent interactions with NECs are required to rescue ATL cells from TSA-induced apoptosis. **A**: Percentage of apoptotic ATL-CR cells. ATL-CR cells were directly co-cultured with HEK293T cells or indirectly co-cultured with HEK293T cells using cell culture inserts (pore size, 0.4 μm) in the presence of the indicated concentrations of TSA for 48 hours. **B**: Means ± SD percentage of ATL-CR cells adhering to HEK293T cells after co-culture for 24 hours. **C**: Most of the ATL-CR cells (red) showed adhesion-dependent growth on a monolayer of HEK293T cells after 24 hours of direct co-culture. Scale bars: 50 μm. **D**: Percentage of apoptotic ATL-CR cells. ATL-CR cells were co-cultured with HEK293T cells in the presence of the indicated concentrations of TSA, VPA, and NaB. After co-culture, nonadhering ATL-CR cells in the supernatant were collected separately from the ATL-CR cells adhering to the monolayer of CFSE-labeled HEK293T cells. The data are presented as the means ± SD of three independent experiments.

contact with HEK293T cells (Figure 2A), indicating that efficient suppression of apoptosis requires cell-cell contact. Approximately 84% of ATL-CR cells adhered to a monolayer of HEK293T cells by 24 hours after co-culture with HEK293T cells (Figure 2, B and C). There was no correlation between the dose of TSA and the adhesiveness of ATL-CR cells (Figure 2B), suggesting that TSA treatment did not augment the adhesive activity of ATL cells. To examine whether the extracellular matrix can substitute for NECs, ATL-CR cells were cultured in an extracellular matrix (BD Matrigel Matrix; Becton Dickinson)—coated dish in the presence of TSA. These experiments showed that extracellular matrix alone was completely ineffective in reducing TSA-induced apoptosis in ATL cells (data not shown).

We next examined whether ATL-CR cells co-cultured with HEK293T cells acquire apoptosis resistance to treatment with other HDAC inhibitors, such as VPA and NaB (Figure 2D). TSA-treated ATL-CR cells directly co-cultured with HEK293T cells acquired dramatic apoptosis resistance regardless of whether they adhered to HEK293T cells. In contrast, apoptosis resistance to VPA or NaB was acquired only in adhering ATL-CR cells, and the extent of acquired resistance was diminished. These results indicate that cell-cell contact—dependent interactions with NECs make ATL-CR cells more or less resistant to apoptosis induced by HDAC inhibitors.

Co-Culture with NECs Induces a Quiescent State in TSA-Treated ATL Cells

To examine the cellular changes that follow co-culture with NECs more closely, we analyzed cell-cycle distribution in ATL cells cultured alone, co-cultured with NECs, or co-cultured with NECs in the presence of TSA (Figure 3A). Co-culture with NECs decreased the proportion of S and G2/M phase cells and increased the proportion of G0/G1 phase cells. Co-culture in the presence of 0.8 μmol/L TSA further strengthened these changes. In contrast, TSA-treated ATL-CR cells cultured alone did not show such cell-cycle changes and underwent apoptosis (Figure 3B). Furthermore, when CFSE-labeled ATL-CR cells were cultured alone or with HEK293T cells for 72 hours, co-cultured ATL-CR cells showed less proliferation than those cultured alone, in the presence and absence of 0.8 μmol/L TSA (Figure 3C). This is consistent with the observation that co-culture with NECs induces G0/G1 accumulation in ATL-CR cells and allows them to escape from TSA-induced apoptosis (Figure 3A).

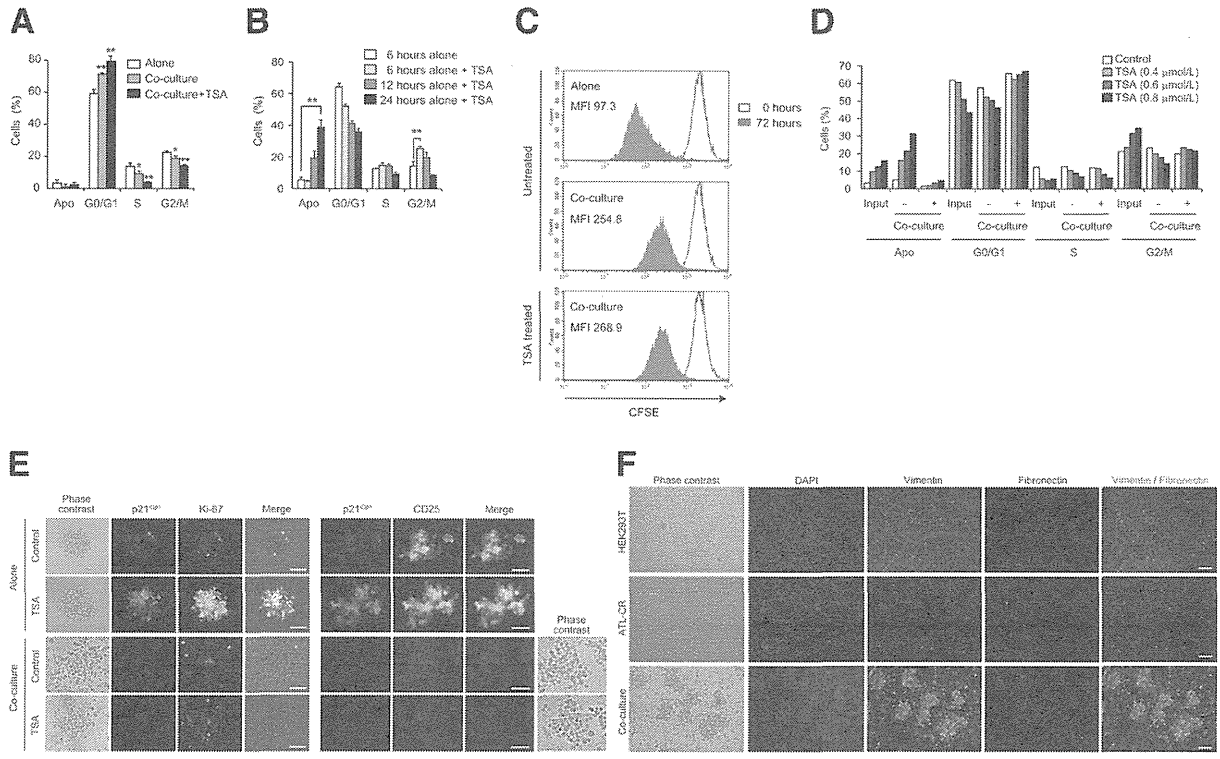

Figure 3 Co-culture with NECs induced a quiescent state in TSA-treated ATL-CR cells. **A**: Cell-cycle analysis in ATL-CR cells. ATL-CR cells co-cultured with HEK293T cells were treated with 0.8 μmol/L TSA for 24 hours. **B**: Changes in cell-cycle distribution were followed for 24 hours in ATL cells cultured alone in the presence or absence of TSA. **C**: Proliferation analysis in ATL-CR cells. CFSE-labeled ATL-CR cells were cultured alone or with HEK293T cells in the presence or absence of TSA for 72 hours. CFSE intensity was analyzed after gating on live cells. **D**: Recovery of TSA-pretreated ATL-CR cells by direct co-culture with NECs. ATL-CR cells were pretreated with the indicated concentration of TSA for 18 hours and then were cultured alone or with HEK293T cells in fresh RPMI 1640 medium for 24 hours. ATL-CR alone (input) indicates TSA-pretreated ATL-CR cells cultured alone. **E**: $p21^{Cip1}$, Ki-67, and CD25 expression in ATL-CR cells. ATL-CR cells were cultured alone or with HEK293T cells in the presence of 0.8 μmol/L TSA. **F**: Expression of vimentin and fibronectin in ATL-CR cells co-cultured with HEK293T cells. Apo, apoptotic cells. The data are presented as means ± SD. $*P < 0.05$, $**P < 0.01$. Scale bars: 50 μm (**E** and **F**).

Next, to examine whether NECs have a protective role on ATL-CR cells pretreated with TSA, ATL-CR cells were incubated with TSA for 18 hours and then were transferred to the fresh medium free of TSA. Pretreatment of ATL-CR cells with TSA increased the proportion of G2/M phase cells in a dose-dependent manner (Figure 3D). These TSA-pretreated cells (shown as input cells) were transferred to the fresh TSA-free medium and were cultured for an additional 24 hours in the presence or absence of HEK293T cells. In the absence of HEK293T cells, the proportion of cells in the G0/G1, S, and G2/M phases continued to decline, and ATL-CR cells continued to undergo apoptosis. In contrast, the ratio of apoptotic cells did not increase appreciably in the presence of HEK293T cells. These results suggest that co-culture with HEK293T cells induced ATL-CR cells to enter the G0/G1 resting phase.

Ki-67 antigen is present during all active phases of the cell cycle (G1, S, G2, and M) but is absent from cells in resting G0 phase. When ATL-CR cells were stained with anti–Ki-67 antibody, most cells were not stained; however, when they were treated with TSA, 44.2% of the cells became positive with Ki-67 and entered the cell cycle (data not shown). TSA increases $p21^{Cip1}$ levels in cancer cells, leading to cell-cycle arrest.[24] When ATL-CR cells cultured alone were treated with TSA, they exhibited markedly induced expression of $p21^{Cip1}$ and Ki-67 and retained high expression of CD25 (Figure 3E). In contrast, when ATL-CR cells were treated with TSA and co-cultured with NECs, expression of $p21^{Cip1}$ and Ki-67 remained low, and expression of CD25 was strongly diminished (Figure 3E).

Vimentin is a mesenchymal intermediate filament supporting the structural integrity of quiescent cells while participating in adhesion, survival, growth regulation, and cell signaling processes.[25] It is a growth-regulated protein whose expression is induced in quiescent cells $\leq$2 hours after mitogenic stimulation, even when protein synthesis is inhibited.[26] We, therefore, examined the expression of vimentin and fibronectin, another mesenchymal marker, in ATL cells adhering to NECs. Expression of vimentin, but not fibronectin, was markedly elevated in ATL-CR cells co-cultured with HEK293T cells (Figure 3F). These results are consistent with the idea that adhesion to NECs induced cellular quiescence and resistance to TSA-induced apoptosis in ATL cells through vimentin expression.

ATL Cells Adhering to NECs Augment CD44 Expression

Cancer stem cell (CSC)–like cells often exhibit markers of epithelial-mesenchymal transition, such as vimentin.[25] Recent evidence indicates that CD44 directly reprograms stem cell properties in colon cancer cells.[27] We, therefore, examined whether the cellular quiescence achieved by co-culture with NECs was accompanied by elevated expression of CD44, a hyaluronan receptor known to be involved in cellular quiescence and now recognized as a marker of CSC-like cells (Figure 4A). When we compared cell surface expression of CD44 on ATL cells co-cultured with NECs and cultured alone in the presence or absence of TSA, CD44 expression was markedly increased in ATL-CR cells co-cultured with HEK293T cells compared with ATL cells cultured alone regardless of the presence or absence of TSA. Staining for CD44 was more pronounced in ATL-CR cells located at the upper and central regions of colonies, whereas vimentin tended to be evenly expressed on all ATL-CR cells (Figure 4, B and C). These observations suggest the involvement of CD44-mediated interactions in the induction of cellular quiescence in co-cultured ATL cells.

ATL Cells that Form Colonies on the Monolayer of NECs Show Intracellular Expression of CD44

ATL cells that formed colonies on the monolayer of NECs were more strongly positive for CD44 than were those that did not form colonies and floated in the medium (Figure 5A). To

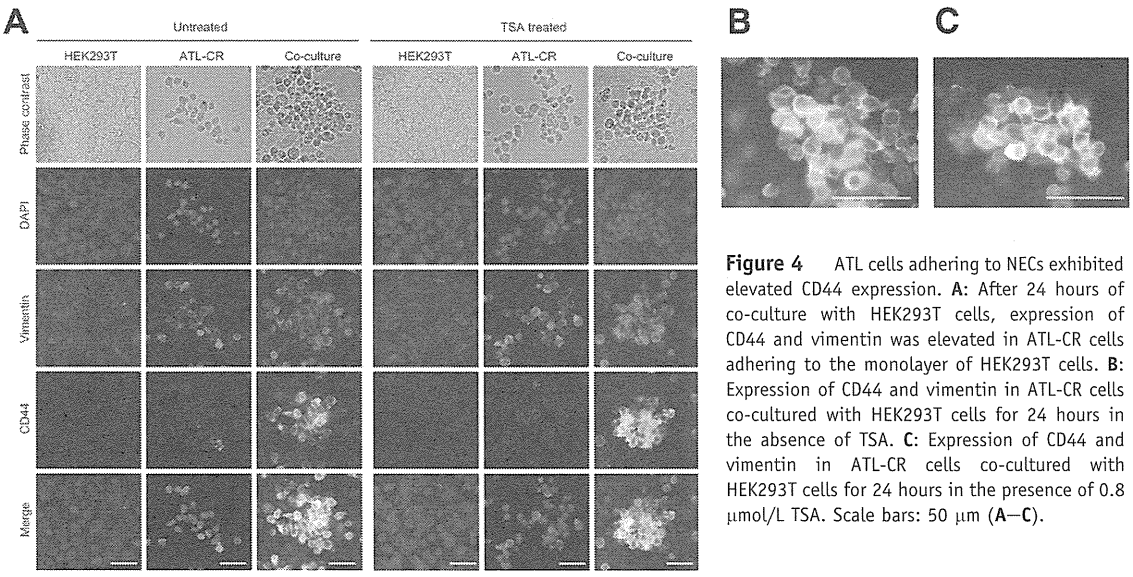

Figure 4 ATL cells adhering to NECs exhibited elevated CD44 expression. **A:** After 24 hours of co-culture with HEK293T cells, expression of CD44 and vimentin was elevated in ATL-CR cells adhering to the monolayer of HEK293T cells. **B:** Expression of CD44 and vimentin in ATL-CR cells co-cultured with HEK293T cells for 24 hours in the absence of TSA. **C:** Expression of CD44 and vimentin in ATL-CR cells co-cultured with HEK293T cells for 24 hours in the presence of 0.8 μmol/L TSA. Scale bars: 50 μm (**A**–**C**).

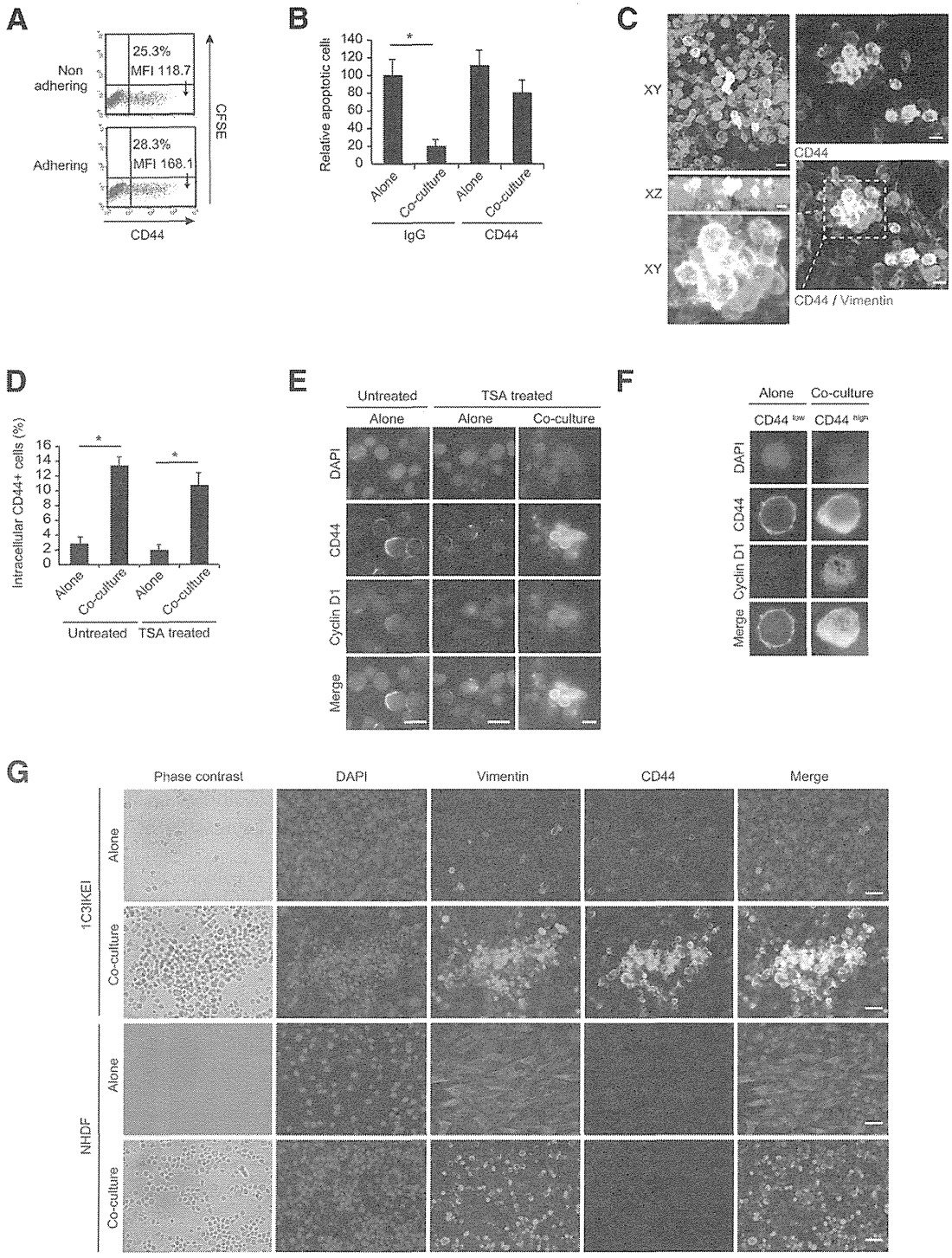

Figure 5 A fraction of ATL cells forming colonies on the monolayer of NECs showed intracellular expression of CD44. **A**: Cell surface expression of CD44 on adhering and nonadhering ATL-CR cells. ATL-CR cells were co-cultured with HEK293T cells for 24 hours. **B**: Blocking antibody for CD44 inhibited the apoptosis-protective effects conferred by co-culture with HEK293T cells. ATL-CR cells cultured alone were pretreated with anti-CD44 antibody or control IgG for 1 hour and then were cultured for an additional 24 hours with or without HEK293T cells in the presence of 0.8 μmol/L TSA. **C**: Three-dimensional analysis by confocal microscopy. Expression of CD44 was observed on ATL-CR cells that formed colonies on the monolayer of HEK293T cells. Expression was particularly pronounced on ATL-CR cells located at the upper and central regions of the colonies. **D**: Percentage of intracellular $CD44^+$ cells. **E**: CD44 and cyclin D1 expression. The TSA concentration used in **D** and **E** was 0.8 μmol/L. **F**: Nuclear localization of cyclin D1 in $CD44^+$ high cells. ATL-CR cells were cultured in the absence of TSA. **G**: CD44 and vimentin expression on ATL-CR cells co-cultured with 1C3IKEI and normal human dermal fibroblast (NHDF) cells. The data are presented as the means ± SD of three independent experiments. $^*P < 0.01$. Scale bars: 10 μm (**C** and **E**); 50 μm (**G**).

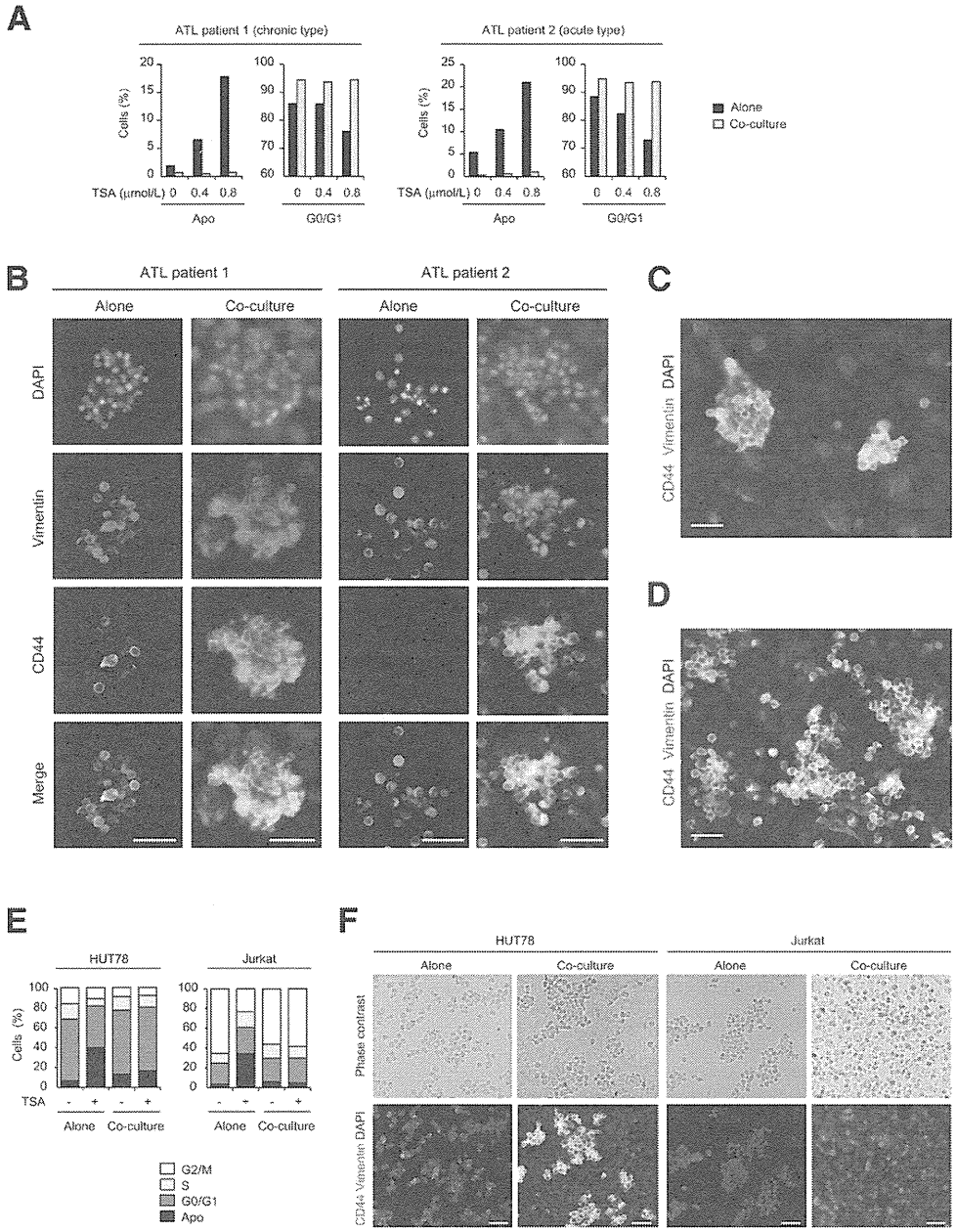

Figure 6 Fresh ATL cells adhering to NECs formed colonies, escaped from TSA-induced apoptosis, and augmented CD44 expression. **A**—**D**: PBMCs derived from patients with ATL with chronic type (patient 1) and acute type (patient 2) were cultured alone or with HEK293T cells with or without 0.8 μmol/L TSA, and then cell-cycle analysis and immunofluorescence staining for CD44 and vimentin were performed. **A**: Percentage of apoptotic cells (Apo) and G0/G1 phase cells. **B**: Expression of CD44 and vimentin in TSA-treated ATL cells. **C** and **D**: Expression of CD44 and vimentin in TSA-untreated ATL cells derived from patient 1 (**C**) and patient 2 (**D**). **E**: Cell-cycle analysis in HTLV-1—negative T-cell lymphoma cells. HUT78 and Jurkat cells co-cultured with HEK293T cells were treated with 0.8 μmol/L TSA for 48 hours. **F**: Expression of CD44 and vimentin was examined in HTLV-1—negative T-cell lymphoma cells co-cultured with HEK293T cells for 24 hours in the presence of 0.8 μmol/L TSA. Scale bars: 50 μm (**B**—**D** and **F**).

examine whether CD44 is involved in apoptosis resistance, we pretreated ATL-CR cells cultured alone with 40 μg/mL of anti-CD44 antibody or control IgG for 1 hour and then cultured for an additional 24 hours in the presence or absence of HEK293T cells (Figure 5B). Treatment with anti-CD44 antibody significantly reduced apoptosis resistance in ATL-CR cells cultured alone and co-cultured with NECs. These results indicate that elevated CD44 expression is involved in conferring apoptosis resistance on TSA-treated ATL-CR cells. Three-dimensional analysis by confocal microscopy revealed a population of ATL cells strongly positive for intracellular CD44; such cells were located on top of colony-forming, vimentin-positive ATL cells (Figure 5C). The proportion of cells showing strong intracellular staining for CD44 was significantly higher in

ATL cells co-cultured with NECs than in ATL cells cultured alone (means ± SD: 10.68% ± 1.65% for TSA-treated co-cultured ATL cells and 1.91% ± 0.47% for TSA-treated ATL cells cultured alone; $P < 0.001$) (Figure 5D).

Recently, it was reported that nuclear translocation of CD44 promotes cell proliferation through direct binding to the promoter region of the cyclin D1 gene.[28] We, therefore, examined whether cells positive for intracellular CD44 express cyclin D1. In TSA-untreated ATL cells, CD44 expression was restricted to the cell surface, with no evidence of nuclear translocation of cyclin D1 (Figure 5E). In TSA-treated ATL cells cultured alone, CD44 surface expression was low, with little detectable nuclear translocation of cyclin D1. In contrast, a fraction of ATL cells co-cultured with NECs was strongly positive for intracellular CD44 and cyclin D1 regardless of whether they were treated with TSA. In ATL cells co-cultured with NECs, nuclear translocation of cyclin D1 was induced after nuclear translocation of CD44 (Figure 5F). These results suggest that nuclear translocation of cyclin D1 enables a fraction of ATL cells to enter the cell cycle from the resting G0/G1 phase, thus accounting for the slower, yet demonstrable cell proliferation observed in Figure 3C.

We confirmed that as in co-culture with HEK293T cells, co-culture with primary epithelial 1C3IKEI cells induced expression of CD44 on a fraction of colony-forming ATL cells (Figure 5G). However, when ATL-CR cells were co-cultured with normal human dermal fibroblasts, they neither formed colonies nor increased CD44 expression (Figure 5G). These results suggest that NECs and fibroblasts confer apoptosis resistance on ATL cells through distinct mechanisms.

Freshly Isolated ATL Cells Form Colonies when Co-Cultured with NECs, Escape TSA-Induced Apoptosis, and Augment CD44 Expression

To assess the clinical relevance of cell-cell interaction between ATL cells and NECs, we isolated PBMCs from two patients with ATL. Patient 1, with chronic-type ATL, had a white blood cell count of 6100/μL, of which 37.3% were lymphocytes. Patient 2, with acute-type ATL, had a white blood cell count of 29,520/μL, of which 88% were lymphocytes. Patient-derived PBMCs were cultured alone or with HEK293T cells with or without 0.8 μmol/L TSA, and then cycle analysis and immunofluorescence staining for CD44 and vimentin were performed. ATL cells co-cultured with HEK293T cells showed no increase in the percentage of apoptotic cells when treated with TSA for 48 hours, indicating that direct co-culture with NECs rescued ATL cells from TSA-induced apoptosis (Figure 6A). When co-cultured with HEK293T cells, a sizable proportion of ATL cells from both patients formed colonies on the monolayer of HEK293T cells and markedly increased CD44 and vimentin expression in the presence (Figure 6B) and absence (Figure 6, C and D) of TSA. Therefore, co-culture with NECs induced similar phenotypic changes in both ATL cell lines and freshly isolated ATL cells.

Next, we examined whether NEC-induced protection occurs in leukemic cells other than ATL cells. When the HTLV-1–negative T-cell lymphoma cells Jurkat and HUT78 were cultured alone in the presence of TSA, they both displayed an increase in the percentage of apoptotic cells, and this increase was abrogated by co-culture with HEK293T cells (Figure 6E). Furthermore, similar to ATL cell lines and freshly isolated ATL cells, HUT78, an epidermotropic HTLV-1–negative T-cell lymphoma cell line established from a patient with Sezary syndrome,[19] formed colonies on the monolayer of HEK293T cells and markedly increased CD44 and vimentin expression (Figure 6F). In contrast, Jurkat cells co-cultured with HEK293T cells neither formed colonies nor increased CD44 expression, suggesting that they presumably escaped from TSA-induced apoptosis by mechanisms distinct from those operating in ATL and HUT78 cells (Figure 6F).

Co-Culture with NECs Reduces the Expression of NKG2D Ligands on ATL-CR Cells

MICA and MICB (MHC class I chain-related proteins A and B) are stress-inducible NKG2D ligands that interact with the activating NKG2D receptor expressed on NK

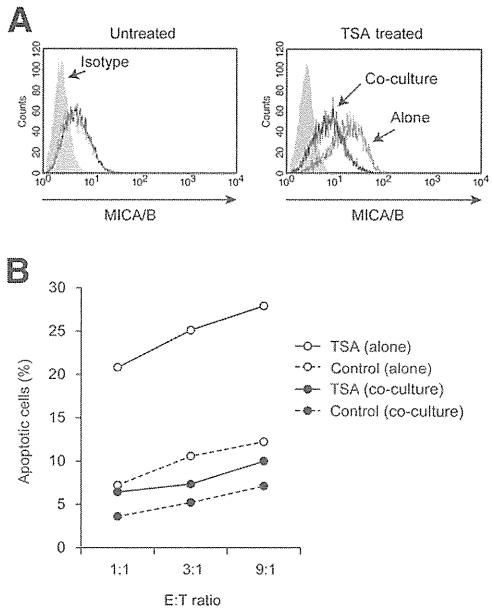

Figure 7 Direct co-culture with NECs reduced the expression of NKG2D ligands on ATL-CR cells. **A:** Induction of MICA/B expression on ATL-CR cells treated with TSA for 18 hours. ATL-CR cells were cultured alone or with HEK293T cells in the presence of 0.2 μmol/L TSA or vehicle. The cell surface expression of MICA/B on ATL-CR cells was analyzed by FCM using an anti-human MICA/B antibody. **B:** Susceptibility of TSA- or vehicle-treated ATL-CR cells to NK cell–mediated cytotoxicity. ATL-CR cells were treated with 0.2 μmol/L TSA or vehicle for 18 hours. CFSE-labeled KHYG-1 cells were used as effector cells and ATL-CR cells as target cells in cytotoxicity assays. Effector cells were incubated with nonlabeled target cells cultured alone or with CFSE-labeled HEK-293T cells at the indicated effector to target cell (E:T) ratios in triplicate wells of 24-well plates for 18 hours. Apoptotic ATL-CR cells were evaluated by FCM for the percentage of sub G0/G1 phase cells in the CFSE-negative cells. The data are presented as the means ± SD of three independent experiments.

cells.[29–31] This interaction activates NK cells, thereby facilitating the elimination of tumor cells. To examine whether co-culture with NECs affects immunologic properties of ATL cells, we cultured ATL-CR cells in the presence or absence of HEK293T cells in a medium containing 0.2 μmol/L TSA and examined MICA/MICB expression on ATL-CR cells. ATL-CR cells co-cultured with HEK293T cells expressed decreased levels of MICA/MICB (Figure 7A). Consistent with this, they became less susceptible to NK cell–mediated cytotoxicity (Figure 7B). These results suggest that interactions with NECs help ATL cells evade NKG2D-mediated immune attack.

Discussion

We demonstrated that in ATL cells cultured alone, TSA treatment induces $p21^{Cip1}$ accumulation, leading to cell-cycle arrest and apoptosis, whereas co-culture with NECs induces G0/G1 accumulation in TSA-treated ATL cells, enabling them to stay in a quiescent state and to acquire apoptosis resistance (Figures 1, 2, and 3). This resistance was acquired even when ATL cells cultured alone were pretreated with TSA and then co-cultured with NECs in fresh TSA-free medium, indicating that the contact with NECs subsequent to exposure to TSA enabled ATL-CR cells that otherwise were destined to undergo apoptosis to recover and resume growth (Figure 3). HDAC inhibitors, such as TSA, VPA, and NaB, induce not only transcriptional activation of viral and host genes but also genomic instability by a variety of mechanisms.[32–34] Thus, the present data suggest that NECs have a key role in guarding ATL cells from genomic instability, including reactivation of viral genes.

Co-culture with NECs induced cellular quiescence in ATL cells as assessed by cell-cycle analysis and staining with Ki-67 (Figure 3). ATL-CR cells that adhered to NECs displayed enhanced expression of CD44 and vimentin (Figures 3, 4, and 5). In this regard, treatment of CSCs with high concentrations of hyaluronan induces cellular quiescence, epithelial-mesenchymal transition, and a multidrug-resistant phenotype.[35] Expression of vimentin and CD44 might be induced by hyaluronan fragments in the extracellular matrix produced by NECs. Accumulating evidence indicates a close link between epithelial-mesenchymal transition and cancer stemness.[25] It is, therefore, possible that direct contact with NECs induces CSC-like phenotypes in ATL cells.

Co-culture with NECs induced expression of CD44 and vimentin in not only ATL cell lines but also ATL cells freshly isolated from patients (Figure 6, A–C), strongly suggesting the potential clinical importance of our observation. Indeed, recent work has shown that CD44 is expressed on skin-infiltrating tumor cells in patients with ATL.[36] Taken together, the present study suggests that interactions with epithelial cells induce CSC-like phenotypes in ATL cells and make them highly resistant to chemotherapies. Co-culture with NECs exerted antiapoptotic effects on two HTLV-1–negative T-cell lymphoma cells, Jurkat and HUT78 (Figure 6E), and induced the expression of CD44 and vimentin in HUT78 cells (Figure 6F). These observations suggest that NECs may play a protective role in lymphomas other than ATL.

Co-culture with NECs reduced expression of the stress-inducible NKG2D ligands MICA and MICB in TSA-treated ATL cells (Figure 7A), presumably because it reduced cellular stresses incurred by epigenetic changes. Reduced MICA and MICB expression made ATL cells less susceptible to cytotoxicity mediated by $NKG2D^{+}$ NK cells (Figure 7B). These results suggest that NECs not only induce CSC-like phenotypes in tissue-infiltrating ATL cells but also facilitate immune evasion by tumor cells.

HDAC inhibitors have emerged as a new class of promising chemotherapeutic agents against cancer.[32] However, monotherapeutic clinical trials with HDAC inhibitors have met with only limited success in most types of cancers.[37,38] The therapeutic efficacy of HDAC inhibitors in patients with ATL is still a controversial issue.[39,40] Furthermore, the safety of this treatment has not been established because it could activate viral genes.[14] The present work suggests that the therapeutic effectiveness of HDAC inhibitors will be reduced against leukemia cells that have invaded epithelial tissues and, thereby, acquired resistance to the inhibitors.

In conclusion, the results of the present study suggest that a propensity of leukemia cells to infiltrate epithelial tissues might produce at least two pathologic outcomes in patients with ATL: survival of leukemia cells through the acquisition of CSC-like phenotypes and evasion of the host immune response through reduced expression of NKG2D ligands.

Acknowledgments

We thank Carlo Bidoia, Virginie W. Gautier, and Noreen Sheehy for helpful discussions, Jonathan Dean for help with FCM analysis, and Masumi Tsuda and Shinya Tanaka for help with confocal microscopic analysis.

References

1. Poiesz BJ, Ruscetti FW, Gazdar AF, Bunn PA, Minna JD, Gallo RC: Detection and isolation of type C retrovirus particles from fresh and cultured lymphocytes of a patient with cutaneous T-cell lymphoma. Proc Natl Acad Sci U S A 1980, 77:7415–7419
2. Yoshida M, Miyoshi I, Hinuma Y: Isolation and characterization of retrovirus from cell lines of human adult T-cell leukemia and its implication in the disease. Proc Natl Acad Sci U S A 1982, 79: 2031–2035
3. Uchiyama T, Yodoi J, Sagawa K, Takatsuki K, Uchino H: Adult T-cell leukemia: clinical and hematologic features of 16 cases. Blood 1977, 50:481–492
4. Bittencourt AL, de Oliveira Mde F: Cutaneous manifestations associated with HTLV-1 infection. Int J Dermatol 2010, 49:1099–1110
5. Ohshima K: Pathological features of diseases associated with human T-cell leukemia virus type I. Cancer Sci 2007, 98:772–778
6. Nasr R, El Hajj H, Kfoury Y, de Thé H, Hermine O, Bazarbachi A: Controversies in targeted therapy of adult T cell leukemia/lymphoma: ON target or OFF target effects? Viruses 2011, 3:750–769

7. Taniguchi Y, Nosaka K, Yasunaga J, Maeda M, Mueller N, Okayama A, Matsuoka M: Silencing of human T-cell leukemia virus type I gene transcription by epigenetic mechanisms. Retrovirology 2005, 2:64
8. Furukawa Y, Osame M, Kubota R, Tara M, Yoshida M: Human T-cell leukemia virus type-1 (HTLV-1) Tax is expressed at the same level in infected cells of HTLV-1-associated myelopathy or tropical spastic paraparesis patients as in asymptomatic carriers but at a lower level in adult T-cell leukemia cells. Blood 1995, 85:1865–1870
9. Gessain A, Louie A, Gout O, Gallo RC, Franchini G: Human T-cell leukemia-lymphoma virus type I (HTLV-I) expression in fresh peripheral blood mononuclear cells from patients with tropical spastic paraparesis/HTLV-I-associated myelopathy. J Virol 1991, 65:1628–1633
10. Nagai K, Jinnai I, Hata T, Usui T, Sasaki D, Tsukasaki K, Sugahara K, Hishikawa Y, Yamada Y, Tanaka Y, Koji T, Mano H, Kamihira S, Tomonaga M: Adhesion-dependent growth of primary adult T cell leukemia cells with down-regulation of HTLV-I p40Tax protein: a novel in vitro model of the growth of acute ATL cells. Int J Hematol 2008, 88:551–564
11. Kinpara S, Hasegawa A, Utsunomiya A, Nishitsuji H, Furukawa H, Masuda T, Kannagi M: Stromal cell-mediated suppression of human T-cell leukemia virus type 1 expression in vitro and in vivo by type I interferon. J Virol 2009, 83:5101–5108
12. Michael B, Nair AM, Datta A, Hiraragi H, Ratner L, Lairmore MD: Histone acetyltransferase (HAT) activity of p300 modulates human T lymphotropic virus type 1 p30II-mediated repression of LTR transcriptional activity. Virology 2006, 354:225–239
13. Ego T, Ariumi Y, Shimotohno K: The interaction of HTLV-1 Tax with HDAC1 negatively regulates the viral gene expression. Oncogene 2002, 21:7241–7246
14. Mosley AJ, Meekings KN, McCarthy C, Shepherd D, Cerundolo V, Mazitschek R, Tanaka Y, Taylor GP, Bangham CR: Histone deacetylase inhibitors increase virus gene expression but decrease CD8+ cell antiviral function in HTLV-1 infection. Blood 2006, 108:3801–3807
15. Panayiotidis P, Jones D, Ganeshaguru K, Foroni L, Hoffbrand AV: Human bone marrow stromal cells prevent apoptosis and support the survival of chronic lymphocytic leukaemia cells in vitro. Br J Haematol 1996, 92:97–103
16. Lagneaux L, Delforge A, Bron D, De Bruyn C, Stryckmans P: Chronic lymphocytic leukemic B cells but not normal B cells are rescued from apoptosis by contact with normal bone marrow stromal cells. Blood 1998, 91:2387–2396
17. Burger JA, Tsukada N, Burger M, Zvaifler NJ, Dell'Aquila M, Kipps TJ: Blood-derived nurse-like cells protect chronic lymphocytic leukemia B cells from spontaneous apoptosis through stromal cell-derived factor-1. Blood 2000, 96:2655–2663
18. Kawaguchi A, Orba Y, Kimura T, Iha H, Ogata M, Tsuji T, Ainai A, Sata T, Okamoto T, Hall WW, Sawa H, Hasegawa H: Inhibition of the SDF-1alpha-CXCR4 axis by the CXCR4 antagonist AMD3100 suppresses the migration of cultured cells from ATL patients and murine lymphoblastoid cells from HTLV-I Tax transgenic mice. Blood 2009, 114:2961–2968
19. Wayner EA, Gil SG, Murphy GF, Wilke MS, Carter WG: Epiligrin, a component of epithelial basement membranes, is an adhesive ligand for alpha 3 beta 1 positive T lymphocytes. J Cell Biol 1993, 121:1141–1152
20. Suck G, Branch DR, Smyth MJ, Miller RG, Vergidis J, Fahim S, Keating A: KHYG-1, a model for the study of enhanced natural killer cell cytotoxicity. Exp Hematol 2005, 33:1160–1171
21. Sheehy N, Lillis L, Watters K, Lewis M, Gautier V, Hall WW: Functional analysis of human T lymphotropic virus type 2 Tax proteins. Retrovirology 2006, 3:20
22. Green KJ, Rowbottom DG: Exercise-induced changes to in vitro T-lymphocyte mitogen responses using CFSE. J Appl Physiol 2003, 95:57–63
23. Schneider CA, Rasband WS, Eliceiri KW: NIH Image to ImageJ: 25 years of image analysis. Nat Methods 2012, 9:671–675
24. Sowa Y, Orita T, Minamikawa-Hiranabe S, Mizuno T, Nomura H, Sakai T: Sp3, but not Sp1, mediates the transcriptional activation of the p21/WAF1/Cip1 gene promoter by histone deacetylase inhibitor. Cancer Res 1999, 59:4266–4270
25. Mani SA, Guo W, Liao MJ, Eaton EN, Ayyanan A, Zhou AY, Brooks M, Reinhard F, Zhang CC, Shipitsin M, Campbell LL, Polyak K, Brisken C, Yang J, Weinberg RA: The epithelial-mesenchymal transition generates cells with properties of stem cells. Cell 2008, 133:704–715
26. Ferrari S, Battini R, Kaczmarek L, Rittling S, Calabretta B, de Riel JK, Philiponis V, Wei JF, Baserga R: Coding sequence and growth regulation of the human vimentin gene. Mol Cell Biol 1986, 6:3614–3620
27. Su YJ, Lai HM, Chang YW, Chen GY, Lee JL: Direct reprogramming of stem cell properties in colon cancer cells by CD44. EMBO J 2011, 30:3186–3199
28. Lee JL, Wang MJ, Chen JY: Acetylation and activation of STAT3 mediated by nuclear translocation of CD44. J Cell Biol 2009, 185: 949–957
29. Gleimer M, Parham P: Stress management: MHC class I and class I like molecules as reporters of cellular stress. Immunity 2003, 19:469–477
30. Raulet DH, Guerra N: Oncogenic stress sensed by the immune system: role of natural killer cell receptors. Nat Rev Immunol 2009, 9:568–580
31. Bauer S, Groh V, Wu J, Steinle A, Phillips JH, Lanier LL, Spies T: Activation of NK cells and T cells by NKG2D, a receptor for stress inducible MICA. Science 1999, 285:727–729
32. Marks PA, Richon VM, Rifkind RA: Histone deacetylase inhibitors: inducers of differentiation or apoptosis of transformed cells. J Natl Cancer Inst 2000, 92:1210–1216
33. Shakespear MR, Halili MA, Irvine KM, Fairlie DP, Sweet MJ: Histone deacetylases as regulators of inflammation and immunity. Trends Immunol 2011, 32:335–343
34. Eot-Houllier G, Fulcrand G, Magnaghi-Jaulin L, Jaulin C: Histone deacetylase inhibitors and genomic instability. Cancer Lett 2009, 274: 169–176
35. Solis MA, Chen YH, Wong TY, Bittencourt VZ, Lin YC, Huang LL: Hyaluronan regulates cell behavior: a potential niche matrix for stem cells. Biochem Res Int 2012, 2012:346972
36. Chagan-Yasutan H, Tsukasaki K, Takahashi Y, Oguma S, Harigae H, Ishii N, Zhang J, Fukumoto M, Hattori T: Involvement of osteopontin and its signaling molecule CD44 in clinicopathological features of adult T cell leukemia. Leuk Res 2011, 35:1484–1490
37. Olsen EA, Kim YH, Kuzel TM, Pacheco TR, Foss FM, Parker S, Frankel SR, Chen C, Ricker JL, Arduino JM, Duvic M: Phase IIb multicenter trial of vorinostat in patients with persistent, progressive, or treatment refractory cutaneous T-cell lymphoma. J Clin Oncol 2007, 25:3109–3115
38. Piekarz RL, Frye R, Prince HM, Kirschbaum MH, Zain J, Allen SL, Jaffe ES, Ling A, Turner M, Peer CJ, Figg WD, Steinberg SM, Smith S, Joske D, Lewis I, Hutchins L, Craig M, Fojo AT, Wright JJ, Bates SE: Phase 2 trial of romidepsin in patients with peripheral T-cell lymphoma. Blood 2011, 117:5827–5834
39. Nishioka C, Ikezoe T, Yang J, Komatsu N, Bandobashi K, Taniguchi A, Kuwayama Y, Togitani K, Koeffler HP, Taguchi H: Histone deacetylase inhibitors induce growth arrest and apoptosis of HTLV-1-infected T-cells via blockade of signaling by nuclear factor kappaB. Leuk Res 2008, 32:287–296
40. Hasegawa H, Yamada Y, Tsukasaki K, Mori N, Tsuruda K, Sasaki D, Usui T, Osaka A, Atogami S, Ishikawa C, Machijima Y, Sawada S, Hayashi T, Miyazaki Y, Kamihira S: LBH589, a deacetylase inhibitor, induces apoptosis in adult T-cell leukemia/lymphoma cells via activation of a novel RAIDD-caspase-2 pathway. Leukemia 2011, 25:575–587

Regular Article

LYMPHOID NEOPLASIA

An animal model of adult T-cell leukemia: humanized mice with HTLV-1–specific immunity

Kenta Tezuka, Runze Xun, Mami Tei, Takaharu Ueno, Masakazu Tanaka, Norihiro Takenouchi, and Jun-ichi Fujisawa

Department of Microbiology, Kansai Medical University, Hirakata, Osaka, Japan

Key Points

- Humanized mice, IBMI-huNOG, were generated by intra–bone marrow injection of human CD133$^+$ hematopoietic stem cells.
- HTLV-1–infected IBMI-huNOG mice recapitulated distinct ATL-like symptoms as well as HTLV-1–specific adaptive immune responses.

Human T-cell leukemia virus type 1 (HTLV-1) is causally associated with adult T-cell leukemia (ATL), an aggressive T-cell malignancy with a poor prognosis. To elucidate ATL pathogenesis in vivo, a variety of animal models have been established; however, the mechanisms driving this disorder remain poorly understood due to deficiencies in each of these animal models. Here, we report a novel HTLV-1–infected humanized mouse model generated by intra–bone marrow injection of human CD133$^+$ stem cells into NOD/Shi-scid/IL-2Rγc null (NOG) mice (IBMI-huNOG mice). Upon infection, the number of CD4$^+$ human T cells in the periphery increased rapidly, and atypical lymphocytes with lobulated nuclei resembling ATL-specific flower cells were observed 4 to 5 months after infection. Proliferation was seen in both CD25$^-$ and CD25$^+$ CD4 T cells with identical proviral integration sites; however, a limited number of CD25$^+$-infected T-cell clones eventually dominated, indicating an association between clonal selection of infected T cells and expression of CD25. Additionally, HTLV-1–specific adaptive immune responses were induced in infected mice and might be involved in the control of HTLV-1–infected cells. Thus, the HTLV-1–infected IBMI-huNOG mouse model successfully recapitulated the development of ATL and may serve as an important tool for investigating in vivo mechanisms of ATL leukemogenesis and evaluating anti-ATL drug and vaccine candidates. (*Blood*. 2014;123(3):346-355)

Introduction

Human T-cell leukemia virus type 1 (HTLV-1) is a retrovirus associated with adult T-cell leukemia (ATL) and HTLV-1–associated myelopathy or tropical spastic paraparesis (HAM/TSP) in humans.[1-3] Although the majority of HTLV-1–infected individuals remain asymptomatic throughout their lives, approximately 5% of HTLV-1 carriers develop ATL or HAM/TSP following a long latency period.[4] In addition to the classic structural proteins required for retroviral replication, the HTLV-1 proviral genome encodes several accessory and regulatory proteins, including the viral transcriptional activator Tax and the HTLV-1 bZIP factor (HBZ), which are thought to be linked to HTLV-1 pathogenesis.[5,6]

ATL is an aggressive malignancy of mature CD4 T cells, characterized by frequent visceral involvement, lymphadenopathy, hypercalcemia or hypercytokinemia, and monoclonal proliferation of HTLV-1–infected tumor cells.[7] Typical ATL cells exhibit an unusual morphology with lobulated nuclei, known as "flower cells."[8] These cells are also characterized by their robust expression of interleukin (IL)-2 receptor α (CD25).[9]

To reproduce the pathogenesis of ATL, a number of mouse models have been developed, including transgenic or xenografted/humanized mice.[10-18] One such model is the Tax-transgenic mouse, which expresses Tax under the control of the Lck promoter. This model restricts Tax expression to developing thymocytes, resulting in characteristic ATL-like phenotypes.[15] Another model, the HBZ-transgenic mouse, expresses HBZ under the control of a CD4-specific promoter/enhancer/silencer. These mice develop lymphomas characterized by induction of Foxp3 in CD4 T cells, similar to leukemic cells in ATL patients.[18] These observations clearly demonstrate that the leukemogenic activity of not only Tax but also HBZ is related to the development of ATL.

In addition to transgenic mouse models, a variety of HTLV-1–infected small-animal models have been established to evaluate viral pathogenesis and elucidate the function of viral products in vivo.[19,20] These infection models have provided valuable findings regarding virus-host interactions; however, they are unable to fully recapitulate pathological conditions resembling ATL, likely due to the low efficiency of HTLV-1 infection.

Humanized mice are highly susceptible to infection with human lymphotropic viruses such as EBV, HIV-1, and HTLV-1, and have been used to recapitulate specific disorders and human immune responses.[17,21,22] Recent studies on HTLV-1 infection in humanized mouse models successfully reproduced HTLV-1–associated T-cell lymphomas[16,17]; however, these models did not accurately recreate human immune responses against HTLV-1.

Submitted June 17, 2013; accepted October 27, 2013. Prepublished online as *Blood* First Edition paper, November 6, 2013; DOI 10.1182/blood-2013-06-508861.

The online version of this article contains a data supplement.

There is an Inside *Blood* commentary on this article in this issue.

The publication costs of this article were defrayed in part by page charge payment. Therefore, and solely to indicate this fact, this article is hereby marked "advertisement" in accordance with 18 USC section 1734.

Notably, humoral immunity, along with cytotoxic T cell (CTL)-mediated cytotoxicity, is thought to play a pivotal role in controlling the proliferation or selection of HTLV-1–infected T-cell clones in vivo.[23,24] It is therefore important to develop mouse models of ATL that induce more human-like HTLV-1–specific immune responses.

In this study, we describe a novel humanized mouse model of HTLV-1 infection in the presence of specific adaptive immune responses. Our novel HTLV-1–infected humanized mice displayed distinct ATL-like symptoms, including hepatosplenomegaly, hypercytokinemia, oligoclonal proliferation of HTLV-1–infected T cells, and the appearance of flower cells. In addition, HTLV-1–specific immunity was induced and may be involved in the control of infected cells in vivo.

Materials and methods

Purification of human CD133$^+$ cells from cord blood

Cord blood samples from full-term human deliveries were obtained from the Japanese Red Cross Kinki Cord Blood Bank (Osaka, Japan) for research use due to the inadequate numbers of stem cells for human transplantation; all patients provided signed, informed consent in accordance with the Declaration of Helsinki. Mononuclear cells (MNCs) were separated using Ficoll-Conray (Lymphosepar I, IBL) density gradient centrifugation. After collecting MNCs, a CD133 MicroBead Kit (Miltenyi Biotec) was used to isolate human CD133$^+$ cells (Miltenyi Biotec) according to the manufacturer's instructions. HLA-A typing was performed using a WAKFlow HLA typing kit (WAKUNAGA) according to the manufacturer's instructions; the results are shown in supplemental Table 1 (available on the *Blood* Web site).

NOG mice

Female 6-week-old NOD/Shi-scid/IL-2Rγc null (NOG) mice[25] were purchased from the Central Institute of Experimental Animals (Kawasaki, Japan). Mice were handled under sterile conditions and were maintained in germ-free isolators. All animal experiments were approved by the Animal Care Committees of Kansai Medical University.

Generation of IBMI-huNOG

Seven-week-old NOG mice were sublethally irradiated with 250 cGy from a ^{137}Cs source (Gammacell 40 exactor, Nordion International). Within 24 hours of irradiation, each mouse was injected with 5×10^4 human CD133$^+$ cells by intra–bone marrow injection (IBMI)[26] as reported previously.[27]

HTLV-1 infection to IBMI-huNOG

The HTLV-1–infected T-cell line MT2[28] was irradiated with 10 Gy from a ^{137}Cs source irradiator. Irradiated MT2 cells (2.5×10^6) or phosphate-buffered saline were inoculated intraperitoneally into 24- to 28-week-old IBMI-huNOG mice. Mice were anesthetized and killed when the body weight decreased to <70% of their maximum weight. Peripheral blood smears were prepared using May-Grunwald Giemsa staining and examined by light microscopy. All infections were performed in a Biosafety Level P2A laboratory in accordance with the guidelines of Kansai Medical University.

Flow cytometric analysis and cell sorting

Peripheral blood cells were routinely collected every 2 weeks after infection, and after sacrificing mice, single-cell suspensions of various lymphoid tissues were prepared as described previously.[29] To stain surface markers, anti–human CD45-PerCP or APC-Cy7, CD3–fluorescein isothiocyanate (FITC) or phycoerythrin (PE)-Cy7, CD4-PE, CD8-PerCP-Cy5.5, CD19-PE, CD25-FITC, CCR4-APC antibodies were used, along with mouse immunoglobllin G1 and FITC as an isotype control (all BD Biosciences). AccuCount Ultra Rainbow Fluorescent Particles (Spherotech) were employed to determine absolute cell numbers, according to the manufacturer's protocol. Flow cytometric analysis was performed on a BD FACSCan for 3-color staining and a BD FACSCant II (BD Biosciences) for 7-color staining. The CellQuest and Diva software programs were used for data acquisition (BD Biosciences), and the collected data were analyzed by FCS express 3 (De Novo Software). Human CD4-, CD8-, and CD25-expressing T cells were sorted from splenic MNCs by FACSAria or FACSAria III (BD Biosciences).

Tetramer staining

PE-conjugated HLA-A*24:02/Tax301-309 (SFHSLHLLF) and HLA-A*24:02/HIV (RYLRDQQLL) env gp160 tetramers were purchased from MBL. Splenocytes from mock-infected or HTLV-1–infected mice were stained with each tetramer and anti–human CD3 and CD8 antibodies according to the manufacturer's protocol. Mixed lymphocyte-peptide cultures were performed to stimulate Tax-specific CTLs, as described previously.[30] Briefly, splenocytes from HTLV-1–infected mice were cultured for 13 days with 10 mg/mL Tax301-309 peptide and 50 U/mL recombinant human IL-2 (Takeda Chemical Industries). Cultured splenocytes were then analyzed by flow cytometry.

DNA isolation and quantification of proviral load

Genomic DNA was extracted from single-cell suspensions of tissue or peripheral blood using a conventional phenol extraction method. Proviral loads (PVLs) were measured by quantitative polymerase chain reaction (PCR) using a MyiQ or CFX96 real-time PCR system (Bio-Rad). The primers and probes targeting for HTLV-1 *pX* and human β-globin (HBB; as a internal control) are listed in supplemental Table 2. A plasmid containing PCR fragments for the HTLV-1 *pX* region and HBB was constructed using T-Vector pMD20 (TaKaRa) and used as the quantified standard template for real-time PCR.[31] The PVL was calculated as: [(copy number of *pX*)/(copy number of HBB / 2)] × 100.

Quantification of clonal occupancy by clone-specific PCR

Inverse long PCR (IL-PCR) was performed to amplify the genomic DNA flanked the 3′ long terminal repeat of HTLV-1 provirus according to a modified method described previously.[32] In brief, the genomic DNA was digested by *Pst*I, self-ligated by T4 ligase, and then digested by *Mlu*I. Long PCR amplification of the linearized DNA was performed using the PrimeSTAR GXL DNA polymerase (TaKaRa) according to the manufacturer's protocol. Primer sets for IL-PCR analysis are listed in supplemental Table 3. IL-PCR products were isolated from agarose gels, purified, and subjected to nested PCR. Amplified nested PCR fragments were subcloned into T-Vector pMD20 (TaKaRa) and sequenced to obtain provirus integration sites downstream of the 3′ long terminal repeat. Integration site-specific primers were designed based on the DNA sequence of the flanking region of the provirus derived from splenic DNA of 8 HTLV-1–infected mice, and are listed in supplemental Table 5. A detailed description of the clone-specific quantitative PCR procedure has been provided elsewhere.[33] The clonal occupancy of each clone was calculated as: [(copy number of integration sites)/(copy number of *pX*)] × 100.

Real-time RT-PCR to quantify *tax* and *HBZ* transcripts

Total RNA was isolated using the TRIzol reagent (Invitrogen) and complementary DNA samples were synthesized from 1 μg total RNA. Reverse-transcription PCR (RT-PCR) was performed by the use of SsoFast EvaGreen Supermix (Bio-Rad). Primers used for RT-PCR are listed in supplemental Table 4. Relative expression levels were calculated by the MyiQ system (Bio-Rad).

Titration of HTLV-1–specific antibodies

The titers of antibodies against HTLV-1 antigens in the plasma of infected mice were determined by the particle agglutination method using Serodia

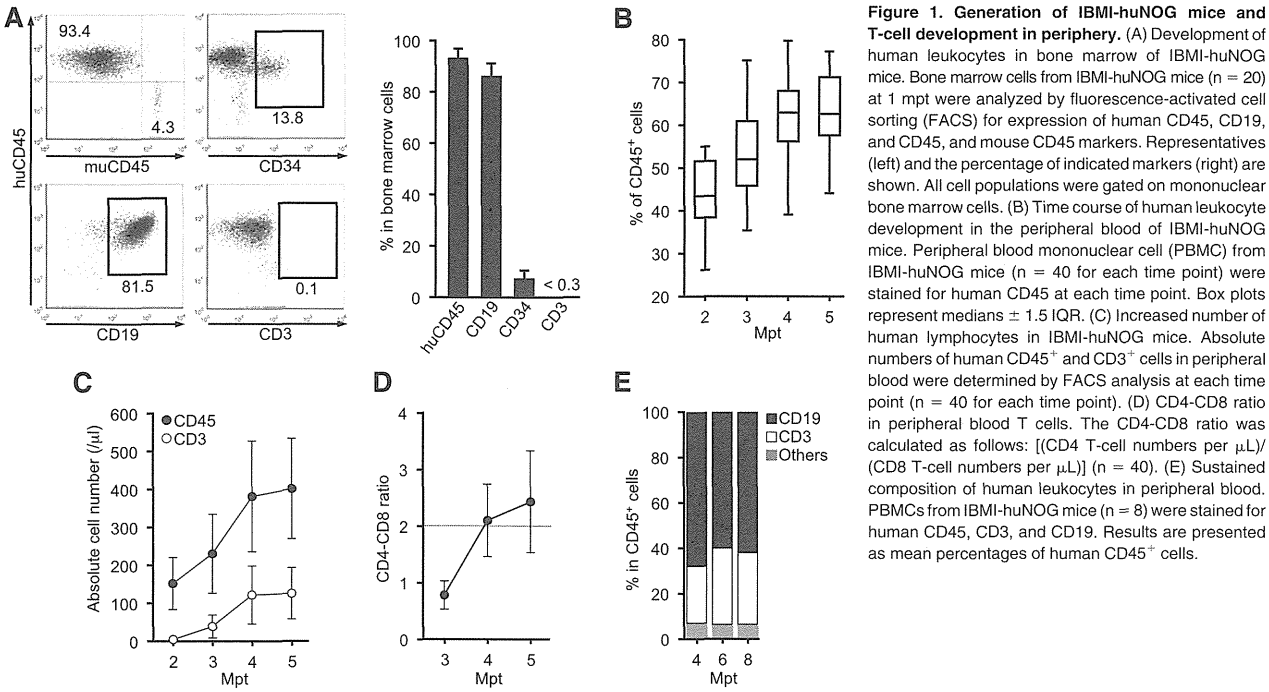

Figure 1. Generation of IBMI-huNOG mice and T-cell development in periphery. (A) Development of human leukocytes in bone marrow of IBMI-huNOG mice. Bone marrow cells from IBMI-huNOG mice (n = 20) at 1 mpt were analyzed by fluorescence-activated cell sorting (FACS) for expression of human CD45, CD19, and CD45, and mouse CD45 markers. Representatives (left) and the percentage of indicated markers (right) are shown. All cell populations were gated on mononuclear bone marrow cells. (B) Time course of human leukocyte development in the peripheral blood of IBMI-huNOG mice. Peripheral blood mononuclear cell (PBMC) from IBMI-huNOG mice (n = 40 for each time point) were stained for human CD45 at each time point. Box plots represent medians ± 1.5 IQR. (C) Increased number of human lymphocytes in IBMI-huNOG mice. Absolute numbers of human $CD45^+$ and $CD3^+$ cells in peripheral blood were determined by FACS analysis at each time point (n = 40 for each time point). (D) CD4-CD8 ratio in peripheral blood T cells. The CD4-CD8 ratio was calculated as follows: [(CD4 T-cell numbers per μL)/(CD8 T-cell numbers per μL)] (n = 40). (E) Sustained composition of human leukocytes in peripheral blood. PBMCs from IBMI-huNOG mice (n = 8) were stained for human CD45, CD3, and CD19. Results are presented as mean percentages of human $CD45^+$ cells.

HTLV-1 (Fuji Rebio).[23] To deplete human immunoglobulin M (IgM) or immunoglobulin G (IgG), streptavidin M-PVA magnetic beads (Chemagen) preincubated with biotin-conjugated goat anti–human IgM or IgG antibody (Sigma-Aldrich) were added to plasma from infected mice; a goat anti–mouse IgG antibody (Organon Teknika) was used as the negative control.

Bio-Plex cytokine assay

Plasma levels of IL-1b, IL-2, IL-4, IL-5, IL-6, IL-7, IL-8, IL-10, IL-12 (p70), IL-13, IL-17, granulocyte colony-stimulating factor (G-CSF), granulocyte macrophage colony-stimulating factor (GM-CSF), interferon-γ (IFN-γ), MCP-1, MIP-1β, and tumor necrosis factor α (TNF-α) in HTLV-1–infected and control mice were analyzed using the Bio-Plex Human Cytokine 17-Plex Panel (Bio-Rad) on a Bio-Plex 200 system according to the manufacturer's instructions.

Statistical analysis

The significance of differences was determined by Mann-Whitney *U* test, paired *t* test, or Spearman's rank-correlation coefficient (*r*); $P < .05$ was considered to indicate statistical significance.

Results

Reconstitution of human immune cells in NOG mice using IBMI

IBMI-huNOG mice were generated by IBMI of human $CD133^+$ hematopoietic stem cells into sublethally irradiated 6- to 7-week-old NOG mice. After 1 month of transplantation, human $CD45^+$ leukocytes were found to have almost completely reconstituted the bone marrow of recipient mice (Figure 1A). At this time point, the majority of the human leukocytes in bone marrow consisted of $CD19^+$ cells. A substantial number of $CD34^+$ cells were also detected, whereas human $CD3^+$ cells had not developed.

Less than half of peripheral blood cells were composed of human leukocytes even at 2 months posttransplantation (mpt). However, the number of human leukocytes increased in a time-dependent manner (Figure 1B-C). Between 3 and 4 mpt, the number of human $CD3^+$ T cells in the peripheral blood increased dramatically, as did the CD4-CD8 ratio (Figure 1D). $CD3^+$ T cells and the CD4-CD8 ratio reached stable levels by 4 to 5 mpt, suggesting that the development of human T cells was completed within this period.

Previous reports have shown that reconstituted human $CD45^+$ cells in other types of humanized mouse systems were overcome by $CD3^+$ T cells within several months of transplantation due to the reduction of B-cell development,[21,34] which may impair the integrity of host immunity. In contrast, the IBMI-huNOG mice model maintained a stable number of $CD3^+$ T cells as well as the B- to T-cell ratio in peripheral blood through at least 8 mpt (Figure 1E). Thus, the human immune system appeared to be effectively reconstituted in IBMI-huNOG mice, likely due to the enriched repopulation of long-term hematopoietic stem cells by direct injection of $CD133^+$ cells into the bone marrow cavity.[27]

Proliferation of HTLV-1–infected T cells in IBMI-huNOG mice

Human T lymphocytes fully developed in IBMI-huNOG mice within 4 to 5 mpt. These mice were then infected with HTLV-1 by intraperitoneal inoculation with 2.5×10^6 irradiated MT2 cells. The number of human $CD45^+$ leukocytes began to increase as early as 4 to 6 weeks postinoculation (wpi) and continued to increase rapidly thereafter (Figure 2A). HTLV-1 infection was also detected by 2 wpi, with the HTLV-1 PVL in peripheral blood increasing in a time-dependent manner (Figure 2B). The proportion of $CD3^+/CD45^+$ T lymphocytes was significantly enriched in HTLV-1–infected mice relative to mock-infected controls (Figure 2C), consistent with previous results.[16] Absence of residual MT2 cells used as the source of HTLV-1 was confirmed by MT2 cell-specific PCR as previously described (supplemental Figure 1).[35]

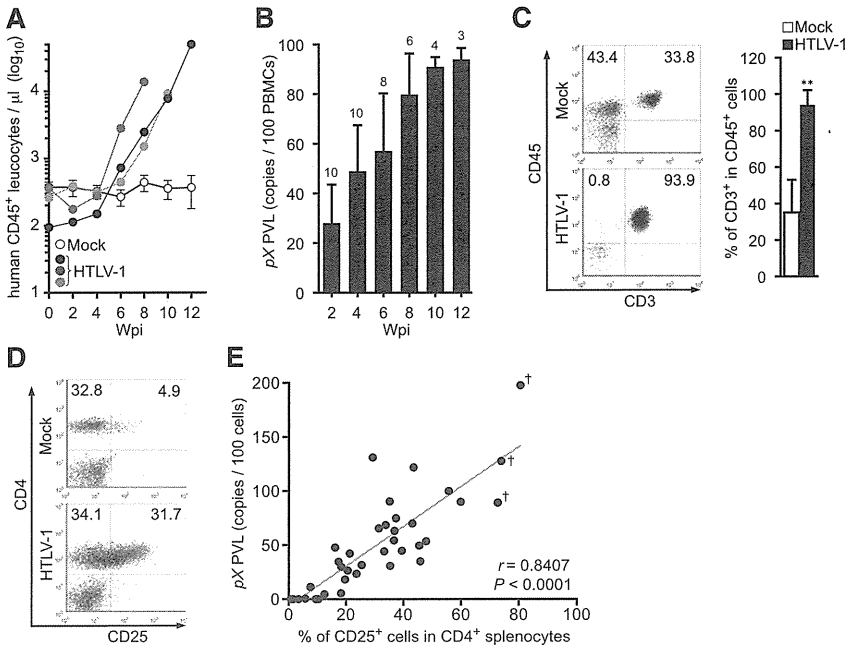

Figure 2. Kinetic analysis of HTLV-1 provirus in infected IBMI-huNOG mice. (A) Quantification of leukocyte numbers in the peripheral blood of HTLV-1–infected mice. Peripheral blood was routinely collected from mock- and HTLV-1–infected mice every 2 weeks. Human CD45$^+$ leukocytes were enumerated by FACS. Results from mock-infected mice (n = 10) are presented as mean ± standard deviation (SD), and representative results of 3 HTLV-1–infected mice are shown. (B) Quantification of HTLV-1 PVL in the peripheral blood of HTLV-1–infected mice. The PVL was determined by real-time PCR. Number at the top of each bar represents the number of analyzed HTLV-1–infected mice at each time point. (C) Expansion of CD3$^+$ T-cell populations in the peripheral blood of HTLV-1–infected mice. PBMCs from mock-infected (n = 3) and HTLV-1–infected mice (n = 18) were stained for human CD3 when sacrificed; the median value was 8 wpi. Results are presented as the average percentages ± SD of human CD45$^+$ cells. (D) Expansion of CD25$^+$ CD4 T cells in the spleen of HTLV-1–infected mice. Splenocytes were stained for human CD3, CD4, and CD25 and analyzed by FACS. Representative results from mock-infected (mouse ID: 8X20) and HTLV-1–infected (mouse ID: 8X01) mice are shown. (E) Correlation between the percentages of CD25$^+$ T cells and PVLs in the spleen. HTLV-1–infected mice (n = 37) were sacrificed to determine PVL and CD25$^+$ T-cell frequency in CD4$^+$ splenocytes. One dot represents the result of an individual HTLV-1–infected mouse. Spearman's rank-correlation coefficient (r) was adopted to identify statistically significant correlations between values. Daggers indicate that flower cells were observed in the peripheral blood of HTLV-1–infected mice.

HTLV-1–infected humanized mice showed marked expansion of CD25$^+$ CD4 T cells in the spleen relative to mock-infected controls (Figure 2D; Table 1), as is observed in peripheral blood of ATL and HAM/TSP patients.[9,36] Furthermore, PVLs in the spleen were significantly correlated with the rate of CD25$^+$ CD4 T cells (Figure 2E). These data suggest that the expanded CD25$^+$ CD4 T-cell population represents the majority of HTLV-1–infected cells in vivo.

ATL-like leukemic symptoms in HTLV-1–infected IBMI-huNOG mice

The majority of HTLV-1–infected mice exhibited splenomegaly, while apparent infiltration of infected T cells in the liver was observed in 3 infected mice with flower cells (Figure 3A; Table 1) and the weight of liver in these mice was remarkably increased (HTLV-1: 1550 ± 620 mg [n = 3]; mock: 715 ± 85 mg [n = 3]). When PVLs of several lymphoid organs were analyzed, the proportions of infected cells in the bone marrow and lymph nodes were significantly lower than those in the spleen and peripheral blood, consistent with the leukemic phenotype of infected mice (Figure 3B). This result is in striking contrast to other humanized mouse models, in which HTLV-1 infection[17] or the ectopic expression of Tax[16] preferentially induce lymphoma.

May-Grunwald Giemsa staining of peripheral blood smears from infected mice revealed the presence of large, abnormal leukemic cells with lobulated nuclei, which were morphologically identical to the flower cells observed in ATL patients (Figure 3D-E).[8] The activated phenotype of infected T cells was also evident, with clear downregulation of CD3 expression on the surface of peripheral T cells in HTLV-1–infected mice, similar to that seen in ATL cells (Figure 3C).[37]

ATL cells have been shown to secrete proinflammatory cytokines, such as IL-6, TNF-α, and GM-CSF, which stimulate activation and proliferation of infected T cells and promote development of ATL leukemogenesis.[38-40] Analysis of cytokine and chemokine levels in the plasma of HTLV-1–infected mice revealed significantly elevated levels of several proinflammatory cytokines (Figure 4). The concentration of IFNγ significantly correlated with PVL in the peripheral blood (supplemental Figure 2), suggesting Th1 immune responses induced in infected mice. Together, these results suggest that HTLV-1–infected IBMI-huNOG mice accurately recreate many of the pathological features of ATL, including hepatosplenomegaly, leukemic T-cell overgrowth with lobulated nuclei, hypercytokinemia, and downregulation of CD3 on T cells.

Oligoclonal proliferation of human T-cell clones in HTLV-1–infected IBMI-huNOG mice

To evaluate the clonal proliferation of HTLV-1–infected T cells in infected mice, we quantified cellular clonality using clone-specific real-time PCR analysis. Splenocytes were isolated from 8 infected mice sacrificed at various time points, and genomic DNA fragments

Table 1. Pathological features of mock- or HTLV-1–infected IBMI-huNOG mice

Mouse ID*	Wpi†	PVL‡	$CD3^+CD4^+$ (%)§	$CD4^+CD25^+$ (%)§	Spleen weight (mg)	Lymph node weight (mg)‖	Observations
8807	—	—	16.7	2.6	45	1	Mock infected
8X10	—	—	20.2	3.4	51	3	Mock infected
8X20	—	—	36.5	4.4	40	2	Mock infected
8401	17	65.6	53.1	31.4	195	23	
8402	11	0.1	5.3	0.7	26	1	
8403	14	0.1	10.8	3.4	35	1	
8404	17	5.4	53.4	18.3	68	2	
8405	12	11.3	30.3	7.6	59	14	
8406	5	0.1	10.5	1.5	33	3	
8407	8	4.5	69.6	12.5	166	9	
8801	25	0.1	59.6	10.4	187	7	
8803	30	0.4	38.6	5.8	55	11	
8804	23	0.1	46.6	9.5	105	5	
8805	8	70.0	57.0	43.1	233	37	Leukemia
8808	8	26.5	52.5	20.6	101	40	
8810	4	42.2	55.4	21.3	40	22	
8X01	5	44.9	65.8	39.5	208	11	
8X04	8	121.9	62.2	43.5	165	7	Leukemia
8X05	23	127.7	81.4	73.9	226	8	Leukemia, flower cells (10.6%),¶ tumor lesion
8X06	9	31.6	50.5	25.5	155	5	
8X09	5	34.6	52.2	17.4	227	9	
8X12	4	47.9	58.5	16.2	188	11	
8X14	25	68.6	51.4	33.8	145	25	Leukemia
8X16	7	90.4	78.9	35.2	200	16	Leukemia
8X17#	9	131.1	44.6	29.3	200	35	Leukemia
8X18	18	197.7	89.4	80.5	358	28	Leukemia, flower cells (19.2%),¶ tumor lesion
9Z01	10	53.6	75.8	47.9	220	12	Leukemia
9Z03	6	23.4	51.6	23.7	38	18	
9Z17	6	18.2	64.7	19.7	163	10	
9Z18	16	89.2	80.4	72.7	285	5	Leukemia, flower cells (4.2%),¶ tumor lesion
9Z19	6	35.0	65.0	45.9	207	20	
X202	12	90.0	76.6	59.9	353	13	Leukemia
X206	8	54.4	56.6	36.7	317	15	
X207**	11	100.0	62.2	55.7	358	6	Leukemia
X208	4	29.9	74.7	18.4	188	15	
X209	7	30.8	74.4	35.4	270	21	
X212	9	74.9	56.8	37.4	270	5	Leukemia
X214	10	44.3	48.0	33.3	170	6	
X216	8	63.2	66.1	36.9	271	12	Leukemia
X217	7	49.6	76.9	45.5	306	18	Leukemia

Leukemia, infected mice with atypical lymphocytes >90% of PBMCs; flower cells, atypical lymphocytes with >4 lobulated nuclei in a cell; tumor lesion, tumor formation of infiltrating infected T cells in the liver.

*The 37 infected mice listed are identical to those in Figure 2E.

†The wpi when indicated mice were sacrificed.

‡PVL is expressed as number of *pX* copies per 100 cells.

§The population of indicated marker-positive cells in $CD45^+$ splenocytes.

‖The weight value of one of the largest mesenteric lymph node in each mouse.

¶The percentage of flower cells in total lymphocytes in blood smear (presented in parentheses).

#High proportion of $CD25^+$ CD8 T cells in PBMCs.

**High proportion of DP T cells in PBMCs.

flanking the major integration sites in the HTLV-1–infected cells were amplified by IL-PCR. Amplified DNA fragments were subcloned into plasmids and sequenced to confirm proper integration (supplemental Table 5). As shown in Figure 5A, the occupancy of detected clones determined by real-time PCR was < 5% in cells harvested 5 to 8 wpi, indicating polyclonal HTLV-1 infection in these mice. In contrast, 2 mice sacrificed after prolonged infection periods (18 and 23 wpi, respectively) produced high percentages of infected clones. Interestingly, these 2 mice also showed overgrowth of $CD25^+$ CD4 T cells with flower-shaped nuclei, characteristic of ATL cells (Figure 3D-E), whereas such cells were not observed in the 6 remaining mice. These findings indicate that a limited number of HTLV-1–infected T-cell clones selectively proliferated in the spleens of infected mice, resulting in an ATL-like leukemic phenotype.[33,41]

Presence of identical infected clones in $CD25^-$ and $CD25^+$ CD4 T-cell populations

Splenocytes from infected mice were sorted into $CD25^-$ or $CD25^+$ CD4 T cells and CD8 T cells; the PVL of each population was also determined. Most of the $CD25^+$ CD4 T cells isolated from the spleens of infected mice were provirus-positive, as was a significant proportion of $CD25^-$ CD4 T cells, whereas infection of CD8 T cells was rare (Figure 5B). Interestingly, *tax* expression in HTLV-1–infected $CD25^+$ CD4 T cells was suppressed compared with that in

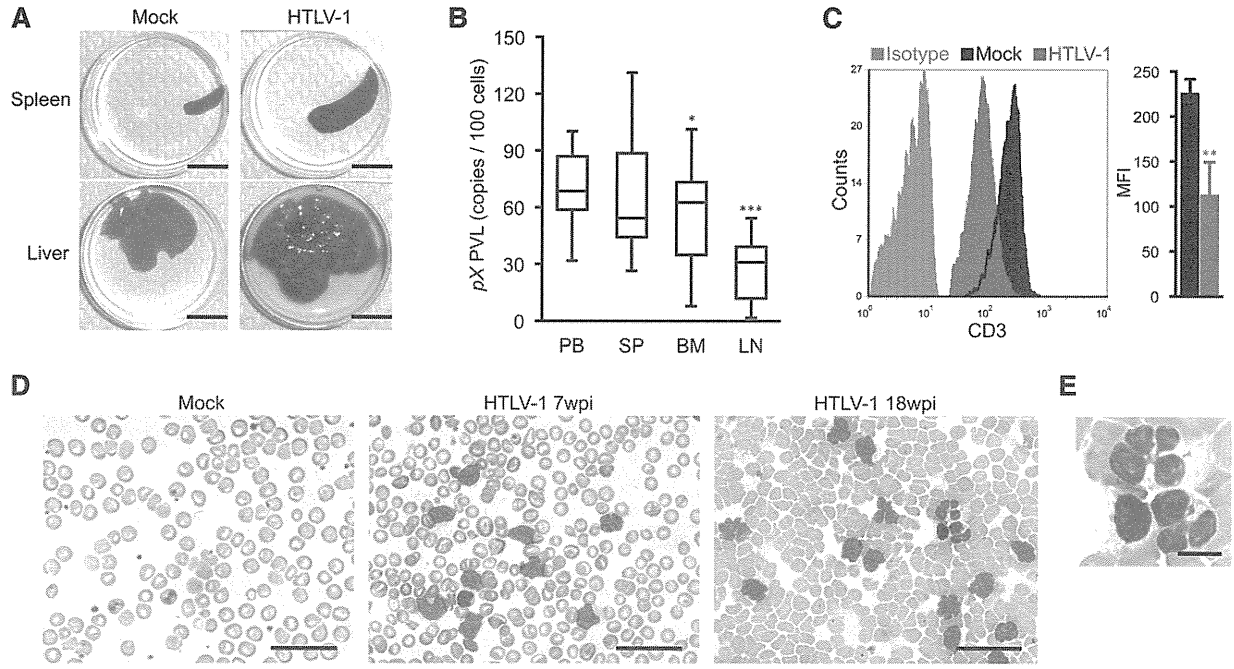

Figure 3. Splenomegaly and leukemic T-cell overgrowth in infected IBMI-huNOG mice. (A) Hepatosplenomegaly in HTLV-1–infected mice. Representative spleens and livers from mock- and HTLV-1–infected mice are shown. Scale bars in panel A represent 10 mm. (B) PVL in lymphoid organs of HTLV-1–infected mice. PVL in the peripheral blood (PB), spleen (SP), bone marrow (BM), and lymph nodes (LM) of HTLV-1–infected mice (n = 17) are shown. Box plots represent medians ± 1.5 IQR. Asterisks indicate statistical significance vs the value obtained from peripheral blood (*$P < .05$, ***$P < .001$ by paired *t* test). (C) Downregulation of CD3 on the T-cell surface. PBMCs from mock- (n = 3) and HTLV-1–infected mice (n = 18) were stained for human CD3 and analyzed by FACS. Results are presented as mean MFI ± SD of CD3 expression. (D-E) Smears of peripheral blood from HTLV-1–infected mice showing a number of leukemic cells with atypically shaped nuclei. Results from two infected mice (7 and 18 wpi, respectively) and a mock-infected mouse (at 8 mpt) are shown. Higher-magnification view of flower cells in panel D is shown in panel E. Scale bars in panels D-E represent 50 and 10 μm, respectively. Asterisks in panels B and C represent significant differences vs mock-infected mice (**$P < .01$ by Mann-Whitney *U* test).

$CD25^-$ CD4 T cells; however, higher *HBZ* expression was observed in $CD25^+$ CD4 T cells (Figure 5C).

Further clonality analysis for HTLV-1–infected $CD25^-$ and $CD25^+$ CD4 T cells isolated from the same spleen with the purity of >95% (supplemental Figure 3) revealed that the most abundant clone was the same in both T-cell populations; however, the occupancy was higher in the $CD25^+$ population (Figure 5D), indicating the preferential growth of infected clones with CD25 expression.

Induction of HTLV-1–specific adaptive immune responses in HTLV-1–infected IBMI-huNOG mice

HLA-A*24:02–restricted Tax-specific CTLs were frequently detected in ATL patients, and are known to play an important role in the control of HTLV-1–infected cells in vivo.[42-44] To investigate whether Tax-specific CTLs were induced in HTLV-1–infected mice, the IBMI-huNOG mice were generated using hematopoietic stem cells purified from the cord blood of an HLA-A*24:02 haplotype individual. HLA-A*24:02 tetramers coupled with Tax301-309 were used to detect CTLs. The cord blood HLA-A alleles used in this study are shown in supplemental Table 1. As shown in Figure 6A, Tax301-309–specific CTLs were detected in HTLV-1–infected mice at a frequency similar to that of ATL patients (0.7% ± 0.8%, n = 18),[45] whereas control tetramer CTLs specific for HIV env produced only marginal staining of CD8 T cells.

To evaluate whether functionally reactive Tax301-309–specific CTLs were present in infected mice, we cultured splenocytes from HTLV-1–infected mice in the presence of Tax peptide. Tax301-309 specific CTLs clearly proliferated following peptide stimulation; no reaction was seen in controls. Furthermore, the frequency of Tax301-309–specific CTLs in in vivo CD8 T cells was inversely correlated with the PVLs of HTLV-1–infected mice (Figure 6B). These results suggest that HTLV-1–infected mice induce functional T-cell–mediated cellular immunity against HTLV-1, which may be involved in the control of HTLV-1–infected cells in vivo.

Antibodies against HTLV-1 antigens were also detected in the plasma of infected mice as early as 2 wpi, whereas the specific antibody was not detected before infection (Figure 6C). The titer of HTLV-1–specific antibodies increased in all cases until 4 wpi, followed by a gradual decline in 67% of infected mice (4 of 6), coincident with a decrease in body weight. However, 2 of the infected mice exhibited a reactivation of antibody production at 8 wpi, suggestive of immunoglobulin class switching from IgM to IgG. In fact, HTLV-1–specific antibody titers were significantly decreased following selective depletion of human IgG, indicating the presence of functional IgG in the plasma of HTLV-1–infected mice (Figure 6D). These data clearly support the notion that the functional interaction between human T and B cells required for class switching exists in this model. Taken together, these results demonstrate that human-like adaptive immunity against HTLV-1 was established in the HTLV-1–infected IBMI-huNOG mice.

Discussion

In this study, we established a novel humanized mouse model of HTLV-1 infection. To generate humanized mice, we transplanted

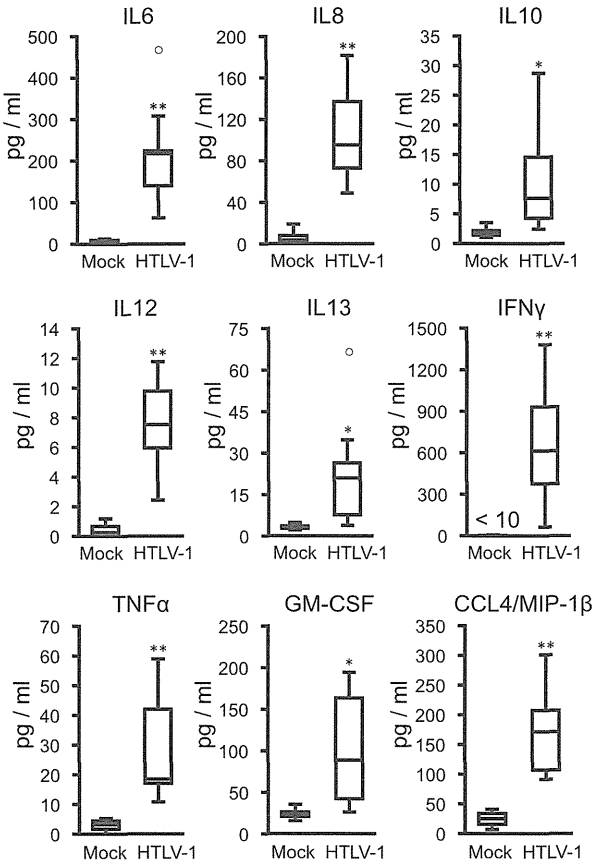

Figure 4. Induction of inflammatory cytokines in infected IBMI-huNOG mice. Human cytokine concentrations in plasma. Plasma was collected following sacrifice of mock-infected (n = 4) and HTLV-1–infected mice (n = 8). Seventeen cytokines were quantified using a cytokine bead array system. The concentrations of human IL-6, IL-8, IL-10, IL-12, IL-13, IFNγ, TNF-α, GM-CSF, and CCL4/MIP-1β are shown, all of which were significantly increased in the plasma of HTLV-1–infected mice. Increased expressions of the other 6 cytokines (IL-2, IL-4, IL-7, IL-17, G-CSF, and MCP-1) were also observed in infected mice but not statistically significant. On the other hand, little decrease in the concentrations of IL-1 and IL-5 was seen. Asterisks in each panel represent significant differences vs mock-infected mice (*$P < .05$, **$P < .01$ by Mann-Whitney U test).

human stem cells directly into the bone marrow cavity of NOD/Shi-SCID/IL-2Rγc null (NOG) mice using an IBMI method.

The efficacy of humanization achieved in this model is markedly superior to other procedures, such as intrahepatic or intravenous injection of human hematopoietic stem cells.[21,22,29] While T-lineage–cell populations become dominant over B-cell populations in the lymphoid organs of other humanized mouse systems within a few months after transplantation, in IBMI-huNOG mice the B-to-T-cell ratio remained constant for >8 months posttransplantation (Figure 1E). One possible explanation for this difference is that direct injection of hematopoietic stem cell preparations into the bone marrow of recipient mice improves the colonization efficiency of long-term stem cells.[27,46] Moreover, we used $CD133^+$ cells to generate IBMI-huNOG mice. CD133, the early hematopoietic progenitor cell marker, is thought to be ancestral to CD34 in human hematopoiesis.[47] Previous studies have revealed that $CD133^+$ cells were capable of differentiating not only into hematopoietic cells but also into endothelial, stromal, neuronal, and other type of cells.[47-49] It is possible that human mesenchymal stromal cells derived from $CD133^+$ cells support the development and maintenance of human B cells in the bone marrow microenvironment.

Having established a new humanized mouse model, we then infected IBMI-huNOG mice with HTLV-1 through inoculation with sublethally irradiated HTLV-1–producing cells.[28] HTLV-1–infected IBMI-huNOG mice recapitulated a large number of pathological features characteristic of ATL patients, including hyperproliferation of $CD3^+$ T cells, clonal proliferation of $CD25^+$ CD4 T cells, the appearance of flower cells in the periphery, hepatosplenomegaly, inflammatory hypercytokinemia, and down-regulation of CD3 on T cells.

Overgrowth of infected T cells was correlated with the expression of CD25 on CD4 T cells, consistent with recent reports.[17] However, the substantial proportion of $CD25^-$ CD4 T cells were also infected and identical T-cell clones, as determined by provirus integration site, were detected as the most abundant clones in both $CD25^-$ and $CD25^+$ CD4 T-cell populations, suggesting that CD25 expression likely occurs after infection in the course of clonal expansion. In addition, the expressions of *tax* and CD25 were inversely correlated. Further research will be necessary to identify molecular events associated with the suppression of *tax* expression in HTLV-1–infected $CD25^+$ CD4 T cells in relation to the development of ATL.

Banerjee et al[16] described the development of T-cell lymphoma following bone marrow transplantation of HTLV-1–infected $CD34^+/CD38^-$ hematopoietic stem cells into a NOD/SCID mouse. The lymphoma cells in these mice were capable of infiltrating into multiple organs but represented only $CD25^-$ or $CD25^{low}$ phenotypes. In contrast, HTLV-1–infected IBMI-huNOG mice developed leukemia in $CD25^+$ CD4 T cells, similar to that observed in ATL patients. The mechanism underlying this difference is unknown but may be due to differences in the developmental stage of T cells at the time of infection. Indeed, HTLV-1 infection in a different humanized mouse model, generated by intrahepatic transplantation of human $CD34^+$ stem cells into $Rag2^{-/-}\gamma c^{-/-}$ mice, induced formation of thymomas/lymphomas in mature CD4 T cells.[17] In this case, HTLV-1 infection was carried out 4 and 8 weeks after transplantation of $CD34^+$ hematopoietic stem cells, giving the human immune system time to develop. Thus the infection of $CD34^+$ stem cells per se does not appear to be sufficient for the induction of mature $CD25^+$ T cell malignancies and may require more developed lymphoid cells or a more appropriate microenvironment capable of supporting cell development.

Furthermore, HTLV-1–infected IBMI-huNOG mice almost exclusively developed leukemia, whereas HTLV-1 infection in the other humanized mouse models described above preferentially induced formation of lymphoma or thymoma. The reason for this difference is not clear but may stem from differences in the timing of T-cell infection. IBMI-huNOG mice were infected after the human hematopoietic system had been fully established, while in the other systems the infection was carried out before or shortly after stem cell transplantation.

In addition to leukemic growth of $CD25^+$ T cells, we also observed formation of flower cells in the peripheral blood of infected mice at later time points postinfection (>16 wpi). Although transformed T cells derived from Tax-transgenic mice were found to exhibit similar morphology,[15] none of the animal models described so far had recapitulated this pathology. Clonal analysis performed as part of this study demonstrated that the expansion of $CD25^+$ T-cell clones preceded the appearance of flower cells in periphery, suggesting a sequence of events that occurs during development of the malignancy. Thus, chronological

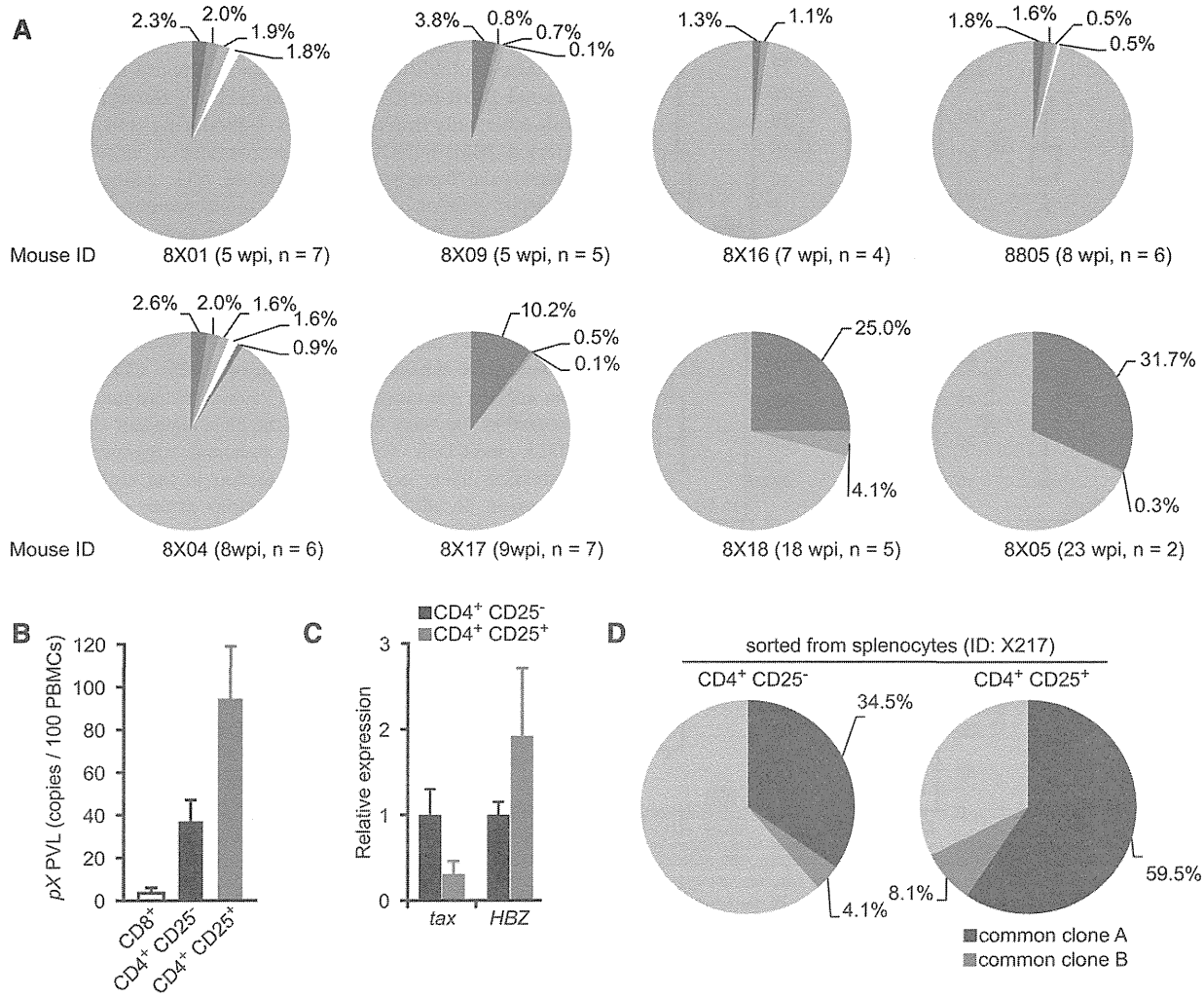

Figure 5. Progression of clonality in splenocytes of infected IBMI-huNOG. (A) Occupancy of HTLV-1–infected clones in the spleen. Abundant integration sites of HTLV-1 provirus were amplified by IL-PCR and subcloned into plasmids. The number of integration sites in each splenic DNA sample was determined by quantitative PCR using the clone-specific nucleotide sequence for each integration site. Results from 8 individual HTLV-1–infected mice are shown as pie charts. Size of the slice is proportional to the relative abundance of T-cell clones successfully amplified by IL-PCR, while data of minor clones with less than 0.1% occupancy were omitted. Gray regions represent clones with undefined integration sites. n, number of integration sites determined by nucleotide sequence of cloned PCR fragments in each mouse. (B) PVLs of specifiedT-cell populations. Splenocytes from HTLV-1–infected mice (n = 5) were sorted into $CD25^-$ or $CD25^+$ CD4 T cells and $CD8^+$ T cells. Genomic DNA isolated from each T-cell population was analyzed for PVL by real-time PCR using primers for the *pX* region of HTLV-1. (C) Comparative analysis of viral transcripts in $CD25^-$ and $CD25^+$ CD4 T-cell populations. Splenocytes from HTLV-1–infected mice (n = 5) are identical to those in mentioned above. The expression levels of *tax* (left) and *HBZ* (right) were analyzed by quantitative RT-PCR and were normalized to that of *HPRT1*. Results are presented as the fold change compared with the value in $CD25^-$ CD4 T cells. (D) Detection of common T-cell clones in the $CD25^-$ and $CD25^+$ CD4 T-cell populations. Clonal occupancy in both $CD25^-$ and $CD25^+$ populations are presented as pie charts. Two abundant common clones were analyzed for occupancy. Identified integration sites are listed in supplemental Table 5. The purity of each sorted population was >95% (supplemental Figure 3).

analysis of genetic and/or biochemical events in infected T cells from this mouse model should provide substantial information regarding the development of ATL.

We detected HLA-restricted CTLs against Tax protein of HTLV-1, as demonstrated in the peripheral blood of HTLV-1–infected carriers,[43] confirming the presence of an acquired immune response. Furthermore, the frequency of CTLs in CD8 T-cell populations were inversely correlated with the number of infected T cells in the spleen of humanized mice, similar to observations in HTLV-1–infected individuals.[43] The presence of functional T cells was also supported by the production of IgG antibodies specific to HTLV-1. Although humanized mice established by the transplantation of $CD34^+$ hematopoietic stem cells have been reported to produce antibodies against specific pathogens such as EBV,[22] HIV-1,[21] and DENV,[50] class switching from IgM to IgG was observed in only a few cases, likely due to immature T-cell development. In the IBMI-huNOG system, however, IgG production against HTLV-1 structural protein was observed after biphasic induction of antibodies after 8 weeks, indicating a functional interaction between CD4 T cells and B cells specific for viral antigens. Taken together, these data demonstrate induction of an adaptive immune response against HTLV-1 in HTLV-1–infected IBMI-huNOG mice, which may play an important role as selective pressure in the expansion of malignant T-cell clones.

In conclusion, our study demonstrates that the HTLV-1–infected IBMI-huNOG mouse represents a novel model that will facilitate elucidation of the molecular mechanism of in vivo development of ATL. Moreover, our model can also be used to develop and evaluate

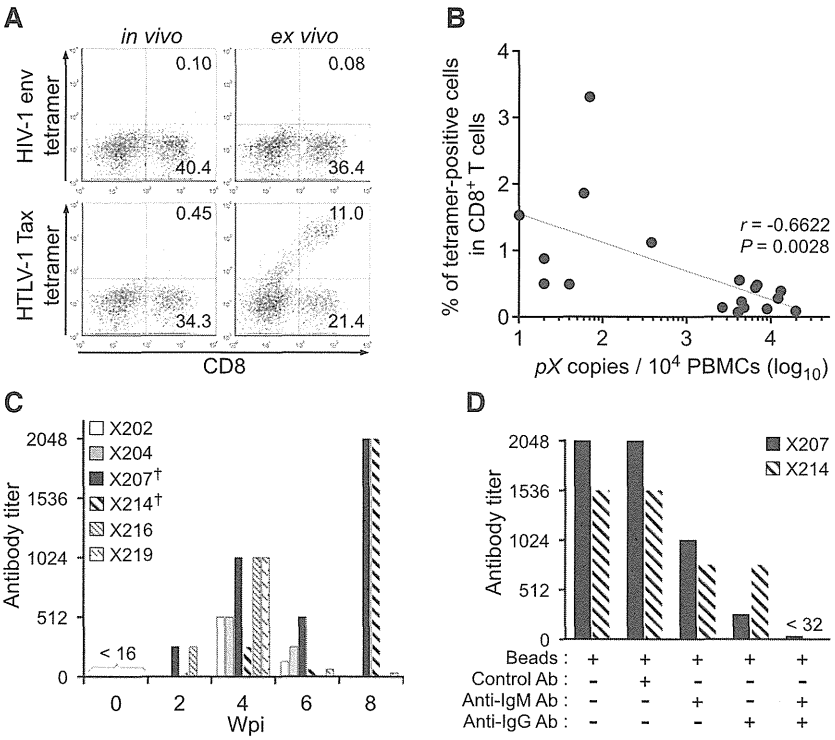

Figure 6. Induction of cellular and humoral immune responses against HTLV-1 in infected IBMI-huNOG mice. (A) Detection of HTLV-1–specific HLA-A*24:02-restricted CTLs. Splenocytes from HTLV-1–infected mice at 8 wpi were stained with human CD8 and Tax301-309 tetramer or HIV-1 env gp160 tetramer as a negative control, respectively. Representative results of tetramer-positive CD8 T cells in vivo (left) and ex vivo culture with Tax peptide (right) are shown. (B) Inverse correlation between PVL and the frequency of Tax301-309–specific CTLs. The percentages of tetramer-positive CD8 T cells and PVL in the spleens of 18 HTLV-1–infected mice are shown. One dot represents the result of an individual HTLV-1–infected mouse. Spearman's rank-correlation coefficient (r^2) was used to identify statistically significant correlations. (C) HTLV-1–specific antibody responses in HTLV-1–infected mice. HTLV-1–specific antibody titers in plasma were monitored by the particle agglutination method. Each bar represents an individual mouse. The plasma of indicated mice prior to infection were used as negative-controls (shown as 0 wpi), and these titers were undetectable level (<16). Mice with daggers (mouse ID: X207 and X214) showed biphasic induction of antibody responses; titers peaked at 8 wpi. (D) Detection of HTLV-1–specific IgM or IgG antibody. Antibody depletion was performed by addition of goat antibodies against human IgG or IgM and anti-goat antibody conjugated magnetic beads to the plasma of two mice, as shown in panel C (indicated by daggers). Bars represent antibody titers in the individual X207 and X214 mice. Ab, antibody.

novel preclinical therapies that target viral gene products or cellular molecules critical for viral replication as well as evaluate the efficacy of vaccine candidates to prevent viral expansion in vivo.

Acknowledgments

The authors thank Drs R. Tatsumi and Y. Adachi for advice in establishing humanized mice and assistance with the pathological analysis, respectively. The authors are grateful to the Japanese Red Cross Kinki Cord Blood Bank for providing the samples used in this study.

This work was supported by Grants-in-Aid for Scientific Research C from the Ministry of Education, Culture, Sports, Science and Technology of Japan (grants 21590515 and 24590562) (J.F.); a MEXT-Supported Program for the Strategic Research Foundation at Private Universities; and Health and Labour Sciences Research Grants for Research on Emerging and Re-emerging Infectious Diseases from Ministry of Health, Labour and Welfare (grant 24171601) (T.U.) (grant 23211801) (M. Tanaka).

Authorship

Contribution: K.T. and J.F. designed the research; K.T. and R.X. established and maintained humanized mice; K.T., R.X., M. Tei and T.U. carried out experiments; M. Tanaka was involved in the IL-PCR analysis; K.T., R.X., M. Tei, and J.F. analyzed results; N.T. performed statistical analysis; K.T. designed the figures; and K.T. and J.F. wrote the paper.

Conflict-of-interest disclosure: The authors declare no competing financial interests.

Correspondence: Jun-ichi Fujisawa, Department of Microbiology, Kansai Medical University, 2-5-1 Shin-machi, Hirakata, Osaka 573-1010, Japan; e-mail: fujisawa@hirakata.kmu.ac.jp.

References

1. Hinuma Y, Nagata K, Hanaoka M, et al. Adult T-cell leukemia: antigen in an ATL cell line and detection of antibodies to the antigen in human sera. *Proc Natl Acad Sci USA.* 1981;78(10):6476-6480.
2. Poiesz BJ, Ruscetti FW, Gazdar AF, Bunn PA, Minna JD, Gallo RC. Detection and isolation of type C retrovirus particles from fresh and cultured lymphocytes of a patient with cutaneous T-cell lymphoma. *Proc Natl Acad Sci USA.* 1980;77(12):7415-7419.
3. Osame M, Usuku K, Izumo S, et al. HTLV-I associated myelopathy, a new clinical entity. *Lancet.* 1986;1(8488):1031-1032.
4. Kondo T, Kono H, Miyamoto N, et al. Age- and sex-specific cumulative rate and risk of ATLL for HTLV-I carriers. *Int J Cancer.* 1989;43(6):1061-1064.
5. Boxus M, Twizere JC, Legros S, Dewulf JF, Kettmann R, Willems L. The HTLV-1 Tax interactome. *Retrovirology.* 2008;5:76.
6. Matsuoka M, Jeang KT. Human T-cell leukemia virus type 1 (HTLV-1) and leukemic transformation: viral infectivity, Tax, HBZ and therapy. *Oncogene.* 2011;30(12):1379-1389.
7. Yoshida M, Seiki M, Yamaguchi K, Takatsuki K. Monoclonal integration of human T-cell leukemia provirus in all primary tumors of adult T-cell leukemia suggests causative role of human T-cell leukemia virus in the disease. *Proc Natl Acad Sci USA.* 1984;81(8):2534-2537.
8. Shimoyama M, Minato K, Tobinai K, et al. Atypical adult T-cell leukemia-lymphoma: diverse clinical manifestations of adult T-cell leukemia-lymphoma. *Jpn J Clin Oncol.* 1983;13(Suppl 2):165-187.
9. Okayama A, Tachibana N, Ishihara S, et al. Increased expression of interleukin-2 receptor alpha on peripheral blood mononuclear cells in HTLV-I tax/rex mRNA-positive asymptomatic carriers. *J Acquir Immune Defic Syndr Hum Retrovirol.* 1997;15(1):70-75.

10. Bieberich CJ, King CM, Tinkle BT, Jay G. A transgenic model of transactivation by the Tax protein of HTLV-I. *Virology.* 1993;196(1):309-318.
11. Feuer G, Zack JA, Harrington WJ Jr, et al. Establishment of human T-cell leukemia virus type I T-cell lymphomas in severe combined immunodeficient mice. *Blood.* 1993;82(3): 722-731.
12. Kondo A, Imada K, Hattori T, et al. A model of in vivo cell proliferation of adult T-cell leukemia. *Blood.* 1993;82(8):2501-2509.
13. Furuta RA, Sugiura K, Kawakita S, Inada T, Ikehara S, Matsuda T, Fujisawa J. Mouse model for the equilibration interaction between the host immune system and human T-cell leukemia virus type 1 gene expression. *J Virol.* 2002;76(6): 2703-2713.
14. Dewan MZ, Terashima K, Taruishi M, et al. Rapid tumor formation of human T-cell leukemia virus type 1-infected cell lines in novel NOD-SCID/ gammac(null) mice: suppression by an inhibitor against NF-kappaB. *J Virol.* 2003;77(9): 5286-5294.
15. Hasegawa H, Sawa H, Lewis MJ, et al. Thymus-derived leukemia-lymphoma in mice transgenic for the Tax gene of human T-lymphotropic virus type I. *Nat Med.* 2006;12(4):466-472.
16. Banerjee P, Tripp A, Lairmore MD, et al. Adult T-cell leukemia/lymphoma development in HTLV-1-infected humanized SCID mice. *Blood.* 2010;115(13):2640-2648.
17. Villaudy J, Wencker M, Gadot N, et al. HTLV-1 propels thymic human T cell development in "human immune system" Rag2$^{-/-}$ gamma c$^{-/-}$ mice. *PLoS Pathog.* 2011;7(9):e1002231.
18. Satou Y, Yasunaga J, Zhao T, et al. HTLV-1 bZIP factor induces T-cell lymphoma and systemic inflammation in vivo. *PLoS Pathog.* 2011;7(2): e1001274.
19. Kazanji M. HTLV type 1 infection in squirrel monkeys (Saimiri sciureus): a promising animal model for HTLV type 1 human infection. *AIDS Res Hum Retroviruses.* 2000;16(16):1741-1746.
20. Lairmore MD, Silverman L, Ratner L. Animal models for human T-lymphotropic virus type 1 (HTLV-1) infection and transformation. *Oncogene.* 2005;24(39):6005-6015.
21. Watanabe S, Terashima K, Ohta S, et al. Hematopoietic stem cell-engrafted NOD/SCID/ IL2Rgamma null mice develop human lymphoid systems and induce long-lasting HIV-1 infection with specific humoral immune responses. *Blood.* 2007;109(1):212-218.
22. Yajima M, Imadome K, Nakagawa A, et al. A new humanized mouse model of Epstein-Barr virus infection that reproduces persistent infection, lymphoproliferative disorder, and cell-mediated and humoral immune responses. *J Infect Dis.* 2008;198(5):673-682.
23. Hasegawa A, Ohashi T, Hanabuchi S, Kato H, Takemura F, Masuda T, Kannagi M. Expansion of human T-cell leukemia virus type 1 (HTLV-1) reservoir in orally infected rats: inverse correlation with HTLV-1-specific cellular immune response. *J Virol.* 2003;77(5):2956-2963.
24. Kannagi M, Hasegawa A, Kinpara S, Shimizu Y, Takamori A, Utsunomiya A. Double control systems for human T-cell leukemia virus type 1 by innate and acquired immunity. *Cancer Sci.* 2011; 102(4):670-676.
25. Ito M, Hiramatsu H, Kobayashi K, et al. NOD/SCID/gamma(c)(null) mouse: an excellent recipient mouse model for engraftment of human cells. *Blood.* 2002;100(9):3175-3182.
26. Kushida T, Inaba M, Hisha H, et al. Intra-bone marrow injection of allogeneic bone marrow cells: a powerful new strategy for treatment of intractable autoimmune diseases in MRL/lpr mice. *Blood.* 2001;97(10):3292-3299.
27. Wang J, Kimura T, Asada R, et al. SCID-repopulating cell activity of human cord blood-derived CD34- cells assured by intra-bone marrow injection. *Blood.* 2003;101(8):2924-2931.
28. Miyoshi I, Kubonishi I, Yoshimoto S, et al. Type C virus particles in a cord T-cell line derived by co-cultivating normal human cord leukocytes and human leukaemic T cells. *Nature.* 1981; 294(5843):770-771.
29. Nie C, Sato K, Misawa N, et al. Selective infection of CD4+ effector memory T lymphocytes leads to preferential depletion of memory T lymphocytes in R5 HIV-1-infected humanized NOD/SCID/IL-2Rgammanull mice. *Virology.* 2009;394(1):64-72.
30. Takamori A, Hasegawa A, Utsunomiya A, et al. Functional impairment of Tax-specific but not cytomegalovirus-specific CD8+ T lymphocytes in a minor population of asymptomatic human T-cell leukemia virus type 1-carriers. *Retrovirology.* 2011;8:100.
31. Ueno S, Umeki K, Takajo I, et al. Proviral loads of human T-lymphotropic virus Type 1 in asymptomatic carriers with different infection routes. *Int J Cancer.* 2012;130(10):2318-2326.
32. Etoh K, Tamiya S, Yamaguchi K, et al. Persistent clonal proliferation of human T-lymphotropic virus type I-infected cells in vivo. *Cancer Res.* 1997; 57(21):4862-4867.
33. Umeki K, Hisada M, Maloney EM, Hanchard B, Okayama A. Proviral loads and clonal expansion of HTLV-1-infected cells following vertical transmission: a 10-year follow-up of children in Jamaica. *Intervirology.* 2009;52(3):115-122.
34. Hiramatsu H, Nishikomori R, Heike T, Ito M, Kobayashi K, Katamura K, Nakahata T. Complete reconstitution of human lymphocytes from cord blood CD34+ cells using the NOD/SCID/ gammacnull mice model. *Blood.* 2003;102(3): 873-880.
35. Nitta T, Tanaka M, Sun B, Hanai S, Miwa M. The genetic background as a determinant of human T-cell leukemia virus type 1 proviral load. *Biochem Biophys Res Commun.* 2003;309(1):161-165.
36. Yamano Y, Araya N, Sato T, et al. Abnormally high levels of virus-infected IFN-gamma+ CCR4+ CD4+ CD25+ T cells in a retrovirus-associated neuroinflammatory disorder. *PLoS ONE.* 2009;4(8):e6517.
37. Matsuda M, Maeda Y, Shirakawa C, et al. CD3 down-regulating factor in sera and culture supernatants of leukaemic cells from patients with adult T cell leukaemia. *Br J Haematol.* 1993;83(2): 212-217.
38. Yamada Y, Ohmoto Y, Hata T, et al. Features of the cytokines secreted by adult T cell leukemia (ATL) cells. *Leuk Lymphoma.* 1996;21(5-6): 443-447.
39. Chiba K, Hashino S, Izumiyama K, Toyoshima N, Suzuki S, Kurosawa M, Asaka M. Multiple osteolytic bone lesions with high serum levels of interleukin-6 and CCL chemokines in a patient with adult T cell leukemia. *Int J Lab Hematol.* 2009;31(3):368-371.
40. Chen J, Petrus M, Bryant BR, et al. Autocrine/ paracrine cytokine stimulation of leukemic cell proliferation in smoldering and chronic adult T-cell leukemia. *Blood.* 2010;116(26):5948-5956.
41. Ohshima K, Mukai Y, Shiraki H, Suzumiya J, Tashiro K, Kikuchi M. Clonal integration and expression of human T-cell lymphotropic virus type I in carriers detected by polymerase chain reaction and inverse PCR. *Am J Hematol.* 1997; 54(4):306-312.
42. Kurihara K, Harashima N, Hanabuchi S, et al. Potential immunogenicity of adult T cell leukemia cells in vivo. *Int J Cancer.* 2005;114(2):257-267.
43. Akimoto M, Kozako T, Sawada T, et al. Anti-HTLV-1 tax antibody and tax-specific cytotoxic T lymphocyte are associated with a reduction in HTLV-1 proviral load in asymptomatic carriers. *J Med Virol.* 2007;79(7):977-986.
44. Harashima N, Kurihara K, Utsunomiya A, et al. Graft-versus-Tax response in adult T-cell leukemia patients after hematopoietic stem cell transplantation. *Cancer Res.* 2004;64(1):391-399.
45. Kozako T, Arima N, Toji S, et al. Reduced frequency, diversity, and function of human T cell leukemia virus type 1-specific CD8+ T cell in adult T cell leukemia patients. *J Immunol.* 2006; 177(8):5718-5726.
46. Nakamura K, Inaba M, Sugiura K, Yoshimura T, Kwon AH, Kamiyama Y, Ikehara S. Enhancement of allogeneic hematopoietic stem cell engraftment and prevention of GVHD by intra-bone marrow bone marrow transplantation plus donor lymphocyte infusion. *Stem Cells.* 2004; 22(2):125-134.
47. Jaatinen T, Hemmoranta H, Hautaniemi S, et al. Global gene expression profile of human cord blood-derived CD133+ cells. *Stem Cells.* 2006; 24(3):631-641.
48. Herrera MB, Bruno S, Buttiglieri S, et al. Isolation and characterization of a stem cell population from adult human liver. *Stem Cells.* 2006;24(12): 2840-2850.
49. Martin-Rendon E, Hale SJ, Ryan D, et al. Transcriptional profiling of human cord blood CD133+ and cultured bone marrow mesenchymal stem cells in response to hypoxia. *Stem Cells.* 2007;25(4):1003-1012.
50. Kuruvilla JG, Troyer RM, Devi S, Akkina R. Dengue virus infection and immune response in humanized RAG2($^{-/-}$)gamma(c)($^{-/-}$) (RAG-hu) mice. *Virology.* 2007;369(1):143-152.